

Effects of chitosan coatings on polypropylene mesh for pelvic floor reconstruction

A Dissertation

Presented to the Faculty of the Graduate School
of Cornell University

In Partial Fulfillment of the Requirements for the Degree of
Doctor of Philosophy

by

Natasha Udpa

January 2014

© 2014 Natasha Udpa

EFFECTS OF CHITOSAN COATINGS ON POLYPROPYLENE MESH FOR PELVIC FLOOR RECONSTRUCTION

Natasha Udpa, Ph. D.
Cornell University 2013

Pelvic floor reconstruction is usually accompanied with the implantation of a surgical mesh, which frequently results in a foreign body response with associated complications. An ideal surgical mesh that allows force generation of muscle tissues without significant granulation tissue and/or fibrosis is of significant clinical interest. In this dissertation, the *in vitro* and *in vivo* responses of a chitosan coating on high molecular weight polypropylene mesh (Ch-PPM) in comparison with commercially available meshes were explored.

In the first study, we found that application of a 0.5% (w/v) Ch-PPM elicited preferential attachment of myoblasts over fibroblast attachment *in vitro*. Therefore, we tested the hypothesis that 0.5% Ch-PPM will encourage skeletal muscle tissue ingrowth and decrease fibrosis formation *in vivo*. In the second topic of investigation, we implanted 0.5% Ch-PPM, collagen-coated polypropylene mesh (Pelvitex™; C.R. Bard), and polypropylene (Avaulta Solo®; C.R. Bard) alone using a rat abdominal defect model. Force generation capacity and inflammatory response of each mesh were

evaluated 2, 4, and 12 weeks post-implantation. We found that chitosan coating is associated with the restoration of functional skeletal muscle with histomorphologic characteristics that resemble native muscle and an early macrophage phenotypic response that has previously been shown to lead to more functional outcomes. Finally, we tested the mesh types in the same *in vivo* rat abdominal defect model to: 1) establish a relationship between the ratio of collagen types I/III and mechanical strength, and 2) determine the collagen deposition and mechanical strength of a chitosan-coated polypropylene mesh. By characterizing the inflammatory response, muscle contractility, and structural properties of mesh types after introduction in a small animal model, we hope to provide more insight for clinicians to reach a more educated decision for selection of a particular material for pelvic floor repair.

BIOGRAPHICAL SKETCH

Natasha Udpa earned her Bachelor of Science in Engineering degree in Mechanical Engineering from the University of Michigan-Ann Arbor in 2008. While at the University of Michigan, Natasha interned with the Harvard-MIT Division of Health Sciences & Technology, Abbott Laboratories, and Ethicon, a subsidiary of Johnson & Johnson. She joined the doctoral program in Mechanical Engineering at Cornell University in 2009 and has since earned her Master of Science degree in Mechanical Engineering in 2012.

In addition to her research experiences, Natasha has been the recipient of the National Science Foundation Graduate Research Fellowship and the Alice H. Cook & Constance E. Cook Award. She was also active in starting the Cornell Graduate Consulting Club, organizing and leading volunteering opportunities as Outreach Director within the SiGMA graduate association, and arranging social events as the Social Chair of the Graduate Women in Science club.

Natasha's dissertation was supervised by Dr. Yingxin Gao.

For Janaki and Vasanthi.

ACKNOWLEDGMENTS

First and foremost, I would like to express my sincere gratitude to my advisor, Professor Gao, for her continuous support, encouragement, friendship, mentorship, and immense knowledge through out my graduate studies. Her editorial advice was essential to the completion of this dissertation and I am privileged to have a rewarding relationship both inside *and* outside the lab with my advisor.

Additionally, thank you to Professors Bonassar and Chu, my PhD committee members, for their guidance in research, collaborations, and teachings. I would also like to thank the National Science Foundation for their extensive support.

This dissertation would not have been possible without the help of so many people in so many ways. Thank you to Janet Snowden at the University of Rochester for helping me get this project started, and to Teresa Porri for her patience and training in the NBTC. I am grateful to John Grazul, John Hunt, and Carol Bayles for their training on the microscopes necessary to complete this research. Thank you to all of my collaborators: Drs. Rohit Rajoria, Helen Valentine, Kate E Breyer, and Bhupinder Singh for their long, painstaking work during surgeries. In particular, I would like to thank Dr. Bryan Brown for his guidance and superb editing during the publication process. Additionally, I am grateful to Dr. Sean McDonough for his collaborative effort and assistance with the histology presented here. To Judy Thoroughman, who responded to—on the order of thousands— of my confused and lengthy emails. And, to Marcia Sawyer, who made MAE feel like a community and has been the pillar of strength for graduate students passing through the hallways of Upson Hall— thank you.

Thank you to Andrea Gerding and Joan Adler who fixed me and put me back together again when I truly needed it. Thank you to *all* my friends in Ithaca, in particular, Santiago, Vlad, Sanjay, Juan, Vic, and Christoffer, for creating a home in a place I never expected to love so dearly. To my labmates: Radhika, Matt, Chi, and Amy for their valuable feedback, edits and support. And to Shama, my labmate/friend/therapist/stats guru, I will miss our long chats in the basement of Weill. To my second set of parents, Lili Mami and Ravi Mama, who gave me confidence that this was research worth pursuing. To my girlfriends: Manwell, Katie, Noopur, Anna, Whitney, and Eden – thank you for the visits, words of encouragement, and memories over the years.

To Anant, who spoiled me rotten while I was a poor graduate student living in Central NY. And, to Keegan, for whom I do not have the verbal prowess to adequately express my thanks, love, gratitude and so much more.

Thank you to my parents and for their love, support, and teaching me the value of an education. Dad, thank you for challenging me *always* to live up to my full potential and reminding me that true accomplishment is how you bounce back after defeat. Momzos, thank you for being my best friend and inspiring me to be a better person and I owe you both everything.

TABLE OF CONTENTS

BIOGRAPHICAL SKETCH	III
ACKNOWLEDGMENTS	V
TABLE OF CONTENTS	VII
LIST OF FIGURES	XI
LIST OF TABLES	XIII
CHAPTER 1: INTRODUCTION	1
1.1 PELVIC CAVITY ANATOMY	1
1.1.1 Bony Scaffolding and Endopelvic Fascia	2
1.1.2 Muscular Supports	2
1.2 INJURY TO THE PELVIC FLOOR	4
1.2.1 Pelvic Floor Disorders (PFDs)	4
1.3 SURGICAL TREATMENT OPTIONS	6
1.3.1 Three Types of Surgical Mesh	6
1.3.2 Surgical Procedures for Pelvic Organ Prolapse (POP)	10
1.4 COMPLICATIONS WITH UROGYNECOLOGIC SURGICAL MESH	11
1.5 EVALUATING UROGYNECOLOGIC MESH ON THE MARKET	12
1.5.1 Evaluation of Biomechanical Properties	12
1.5.2 Histological Outcomes	13

1.6 RE-ESTABLISHING MUSCLE CONTRACTILITY	14
1.7 INTRODUCTION TO CHITOSAN	14
1.8 OVERVIEW AND STUDY OBJECTIVES	16
1.8.1 Objective I	17
1.8.2 Objective II	17
1.8.3 Objective III	18
CHAPTER 2: MEASURING THE ATTACHMENT OF MYOBLASTS ON CHITOSAN-COATED VS. NON-COATED POLYPROPYLENE MESH IN VITRO	20
2.1 INTRODUCTION	20
2.2 MATERIALS AND METHODS	23
2.2.1 Overview of Experimental Design	23
2.2.2 Preparation of Chitosan-coated Meshes and Characterization	23
2.2.3 Overview of in vitro Study	24
2.2.4 In vitro Immunocytochemistry & Co-culture	24
2.2.5 In vitro Characterization of Cell Attachment on Mesh	25
2.2.6 Overview of in vivo Study	26
2.2.7 In vivo Surgical Procedure	26
2.2.8 In situ Force Generation Testing	27
2.2.9 Histology	28

2.2.10 Assessment of Macrophage Phenotype and Expression of Myogenin	31
2.2.11 Statistical Analysis	32
2.3 RESULTS	33
2.3.1 Analysis of Mesh Materials by SEM and Fourier Transformation Infrared Spectroscopy (FTIR)	33
2.3.2 Characterization of Cell Attachment on Mesh using Fluorescent Microscopy	37
2.3.3 Analysis of Force Generation	39
2.3.4 Histopathological Assessment	40
2.3.5 Macrophage Phenotype and Expression of Myogenin	45
2.4 DISCUSSION	47
CHAPTER 3: BIOMECHANICAL PROPERTIES OF MESH MATERIALS FOLLOWING IMPLANTATION IN THE RAT ABDOMINAL WALL MODEL	52
3.1 INTRODUCTION	52
3.2 MATERIALS AND METHODS	55
3.2.1 Overview of Experimental Design	55
3.2.2 Preparation of Chitosan-coated Meshes and Characterization	56
3.2.3 in vivo Surgical Procedure	56
3.2.4 Collagen Typing	57
3.2.5 Uniaxial Tensile Testing	58

3.2.6 Statistical Analysis	60
3.3 RESULTS	60
3.3.1 Analysis of Collagen Typing	60
3.3.3 Analysis of Uniaxial Tensile Testing	63
3.4 DISCUSSION	66
CHAPTER 4: CONCLUSION AND FUTURE WORK	71
4.1. CONCLUSION	71
4.2. FUTURE WORK	76
APPENDIX I: IN VITRO PROTOCOLS	81
APPENDIX II: RAT MODEL PROTOCOLS	93
REFERENCES	98

LIST OF FIGURES

Chapter 1

- Figure 1.1: Transverse plane of pelvic diaphragm 4
- Figure 1.2: A uterine prolapse occurs when a woman's pelvic muscles and ligaments become weak, causing the uterus to drop from its usual position. This allows the neck of the uterus (cervix) to bulge down into the vagina 5
- Figure 1.3: Classification of surgical mesh materials 8
- Figure 1.4: Macroscopic analysis of commercially available mesh 9
- Figure 1.5: Polypropylene mesh is placed over the anterior and posterior vaginal walls and then sutured to the anterior sacrum 11

Chapter 2

- Figure 2.1: Scanning electron microscope (SEM) micrographs of mesh types (A) Avaulta Solo® C.R. Bard, knitted polypropylene mesh (PPM), (B) 0.3% Ch-PPM, (C) 0.5% Ch-PPM, (D) 0.7% Ch-PPM, (E) Pelvitex™, C.R. bard, collagen-coated polypropylene mesh (Col-PPM). Scale bar = 300 mm. Ch-PPM, chitosan-coated PPM. 35
- Figure 2.2: FTIR spectra of high molecular weight chitosan(600,000 MW) and uncoated PPM, 0.3% Ch-PPM, 0.5% Ch-PPM, 0.7% Ch-PPM. FTIR, Fourier transformation infrared spectroscopy. 36
- Figure 2.3: (A) Total number of cells attached to mesh samples. (B) The ratio of myoblast:fibroblast (myo / fb) for mesh samples. The ratio was measured using the DiO:DiI fluorescence ratio. 38
- Figure 2.4: In situ force generation of mesh samples. 39
- Figure 2.5: Comparison of representative tissue reactions to three test mesh articles at 12 weeks of post-implantation. (A) Ch-PPM. (B) PPM (Avaulta Solo, C.R. Bard, Inc.). (C) Col-PPM (Pelvitex; C.R. Bard, Inc.). 42
- Figure 2.6: Tissue reaction over time to Ch-PPM. At 2 weeks (A) and at 12 44

weeks (B).

Figure 2.7: Immunolabeling of macrophage surface markers. Mesh materials were labeled with a pan macrophage marker (CD68, red), an M1 marker (CD86, yellow), and an M2 marker (CD206, green). 46

Figure 2.8: Immunolabeling of monoclonal mouse anti-myogenin of (A) Ch-PPM, (B) PPM, and (C) Col-PPM. 46

Chapter 3

Figure 3.1: Mesh samples explanted after implantation. Visualization by crossed Polaroid filters allowed estimation of collagen type I, seen as thick yellow, orange or red colored fibers and collagen type III fibers are thinner and stained in pale green shades 62

Figure 3.3: Representative stress-strain curve of mesh samples. (A) Ch-PPM, PPM, & Col-PPM at 4 weeks; and at (B) 12 weeks. 65

Chapter 4

Figure 4.1: Histological trichrome images indicating the difference in morphology of the animal model from L to R (A) rat, (B) rabbit, (C) primate, (D) sheep, with respect to humans (E). 77

Figure 4.2: Schematic of a biaxial testing device 79

LIST OF TABLES

Chapter 2

Table 2.1: Method of semi-quantitative histopathological assessment	30
Table 2.2: Mean rounded scores, width of inflammatory response, and width of fibrosis for each implant	41

Chapter 3

Table 3.1: Ratio of collagen I/III ratios in mesh samples	62
Table 3.2: Comparison of tensile properties of neo-tissue after mesh implantation at 4 and 12 weeks	64

Chapter 1

Introduction

Nearly half of the parous women in the U.S. have suffered from some degree of genital prolapse (1,2). Each year, an estimated 135,000 women undergo surgery for urinary incontinence and 225,000 women undergo surgery for pelvic organ prolapse in the United States (3). One in nine American women requires a primary operation for a pelvic floor disorder (PFDs), and almost a third of those women suffer from recurrent prolapse, which requires a second operation. These surgeries and treatment options had a direct cost of over \$1 billion in 1997 in the United States (4). It is expected that urogynecological care will escalate 45% between the years 2000 and 2030 (5).

In this thesis, the effects of chitosan coating on polypropylene mesh samples for pelvic floor reconstruction are investigated. The effective management of PFD and providing proper treatment to women with PFDs requires knowledge of the anatomy and function of the female pelvic floor and its supporting structures.

1.1 Pelvic Cavity Anatomy

The pelvic cavity is defined as the space bounded by the bones of the pelvis and containing the pelvic viscera. The pelvic cavity is made up of the bony structure, endopelvic fascia, and pelvic floor.

1.1.1 Bony Scaffolding and Endopelvic Fascia

The bones that make up the pelvis provide the framework on which the soft tissue supports (muscles, ligaments, and fascia) are attached. The bony pelvis consists of the two hipbones that are fused to the sacrum posteriorly and to each other anteriorly at the pubic symphysis. Each hipbone is composed of the ilium, ischium, and pubis, which are connected by cartilage in young children but fuse together for adults (6).

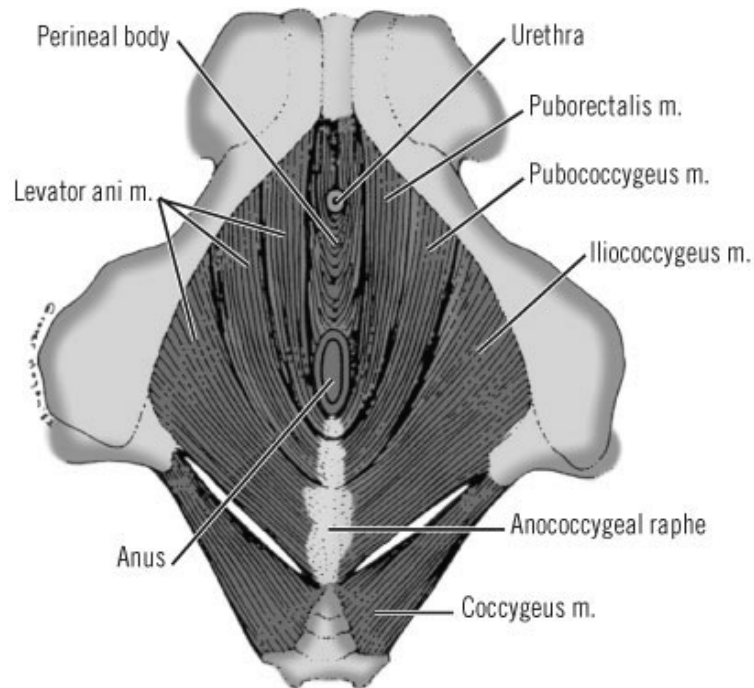
Endopelvic fascia is a network of fibromuscular tissue positioned between the peritoneum and the levator muscles. It surrounds and connects the bladder, uterus, vagina, and rectum to the pelvic walls, so to stabilize the pelvic viscera (7).

1.1.2 Muscular Supports

The pelvic floor is a group of muscles that form a sling or hammock across the opening of a pelvis. These muscles, with surrounding tissues, keep the pelvic organs in place so they can function correctly. The pelvic floor, a three-dimensional structure, works as a unit, and although the muscles are often referred to independently, the boundaries are often difficult to delineate and they perform analogous physiologic functions (7).

The muscles that make up the pelvic floor consist of both type I and type II fibers (7). Type I muscle fibers are slow twitch and provide sustained muscle tone of the pelvic floor. These fibers play a critical role in delivering dynamic pelvic floor support, consequently taking the mechanical stress away from the endopelvic connective tissue attachments. Type II fibers are fast twitch fibers that are responsible for the reflex contractions of the pelvic floor associated with sudden increases in intra-abdominal

pressure (i.e. coughing, childbirth). There are three regions that make up the pelvic floor (Figure 1.1). Region 1 is the pubovisceral muscle, which is comprised of fatigue-resistant (type I) muscle fibers that begin at the pubic bone on both sides of the symphysis and connect to the walls of pelvic organs and the perineal body; these fibers assist in closing the opening in the levator ani through which the urethra and vagina pass, or urogenital hiatus. Region 2, the puborectal muscle, forms a sling around and behind the rectum, just near the external anal sphincter. Region 3 is the iliococcygeal portion, which forms a relatively flat, horizontal shelf spanning the potential gap between pelvic sidewalls and the sacrum (8). The levator ani and coccygeus muscles are attached to the inner surface of the minor pelvis to form the pelvic floor. The pelvic floor fulfills multiple functions. For one, the contraction of the pubococcygeus muscle narrows the genital hiatus. Additionally, contraction of the pelvic floor leads to the elongation and elevation of the pelvic organs allowing for urinary and fecal continence (7).



Copyright ©2006 by The McGraw-Hill Companies, Inc.
All rights reserved.

FIGURE 1.1. Transverse plane of pelvic diaphragm (9)

1.2 Injury to the Pelvic Floor

1.2.1 Pelvic Floor Disorders (PFDs)

A pelvic floor disorder (PFD) occurs when the pelvic muscles and connective tissue in the pelvis weaken or are injured, this causes the pelvic organs to become displaced from their normal anatomical position (Figure 1.2). PFDs often require surgical treatment, necessitating reinforcement of weakened tissues with a surgical mesh material. PFDs consist of a broad range of interrelated clinical conditions including pelvic organ prolapse, urinary incontinence, fecal incontinence, voiding

dysfunction, defecatory dysfunction, and sexual dysfunction (3), and are associated with a negative impact on a woman's social, physical and psychological well-being.

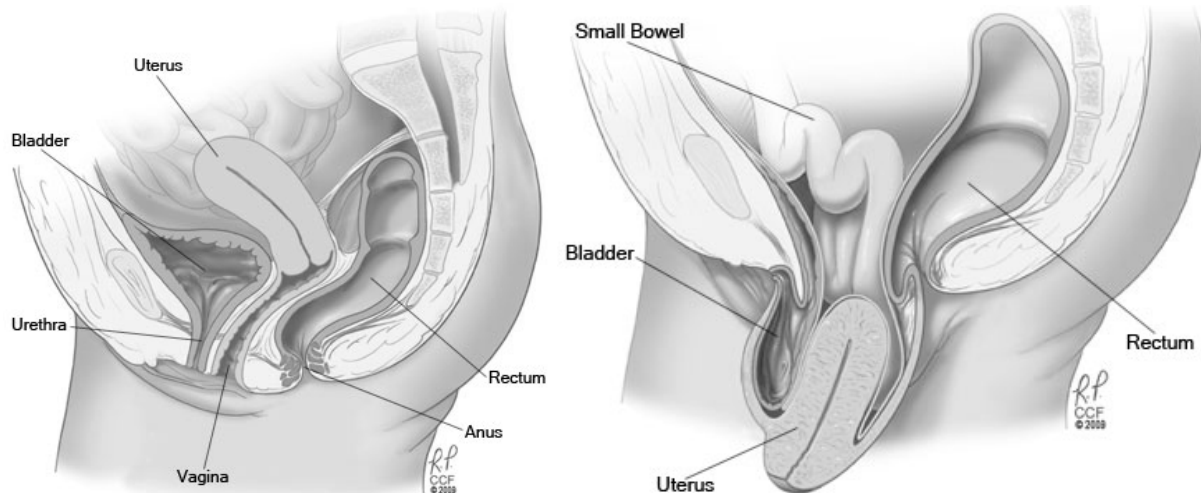


FIGURE 1.2. A uterine prolapse occurs when a woman's pelvic muscles and ligaments become weak, causing the uterus to drop from its usual position. This allows the neck of the uterus (cervix) to bulge down into the vagina (Courtesy of Cleveland Clinic).

Vaginal childbirth, surgical technique, and high body-mass index are the most consistent risk factors, with the number one risk factor being vaginal childbirth (8,10–16). In one study conducted by Ashton-Miller, none of the 80 nulliparous women serving as controls had injuries, thereby identifying birth as a cause of the type of levator ani muscle injury seen in women with pelvic floor dysfunction (8). Biological modifications that occur post-vaginal delivery during reproductive years can lead to increased problems later in their life that result in prolapse of pelvic organs and/or urinary incontinence (8,12,17). Developing a PFD significantly affects women's quality of life and often result in the need for complex surgery that has an unfortunately high reoperation rate of approximately 30% (18).

1.3 Surgical Treatment Options

Surgical management of PFDs have undergone several paradigm shifts over the last few decades (19). In an effort to improve outcomes in transvaginal prolapse repairs, multiple biologic and synthetic graft materials have been introduced to reinforce and/or replace native tissue (2,20). Studies have shown lower failure rates after surgery with urogynecologic mesh, as compared with the traditional repair—also known as native tissue repair—of pelvic organ prolapse (19,21–23). However, as compared with anterior colporrhaphy (repair of the vaginal wall), use of a typical trocar-guided mesh for cystocele repair resulted in higher short-term rates of successful treatment but also in higher rates of surgical complications and postoperative adverse events(21). The following sub-sections take a closer look at the types of mesh on the market and complications associated with them.

1.3.1 Three Types of Surgical Mesh

Women suffering from pelvic organ prolapse who fail or decline pessary usage are candidates for surgical treatment. Reconstructive surgery aims to re-position the prolapsed vaginal canal or organ while alleviating any associated pelvic symptoms (10).

Synthetic, biological and mixed-type mesh are most often used as surgical treatment options (Fig 1.3) (24). Of the synthetic meshes, Type I polypropylene mesh is most commonly used. Polypropylene mesh is the oldest prolapse mesh on the market and has shown favorable clinical efficacy and advantageous tensiometric strength compared with other synthetic meshes (11,25). The permanency of polypropylene

allows mesh to keep its strength for a long period of time. Conversely, macroporous polypropylene mesh has been shown to produce persistent mild inflammatory changes, in comparison with other synthetic meshes (26,27). Biological grafts are usually of either porcine or bovine origin, and mixed-type meshes have a synthetic polypropylene core with a biological collagen wrapping. Animal-derived biological mesh will degrade and lose strength over time. It is not intended to provide long-term reinforcement to the repair site and as a result not commonly seen for pelvic floor repair. As the material degrades, new tissue growth is intended to provide strength to the repair. Mixed-type meshes have a synthetic polypropylene core with a biological collagen wrapping. The morphology of two popular meshes is shown in Fig. 1.4.

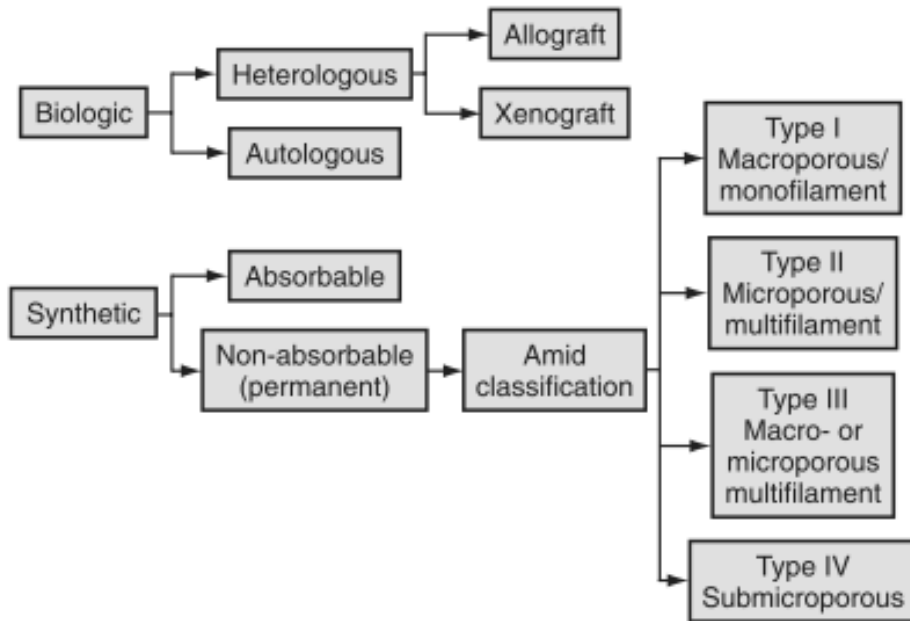


FIGURE 1.3 Classification of surgical mesh materials (7)

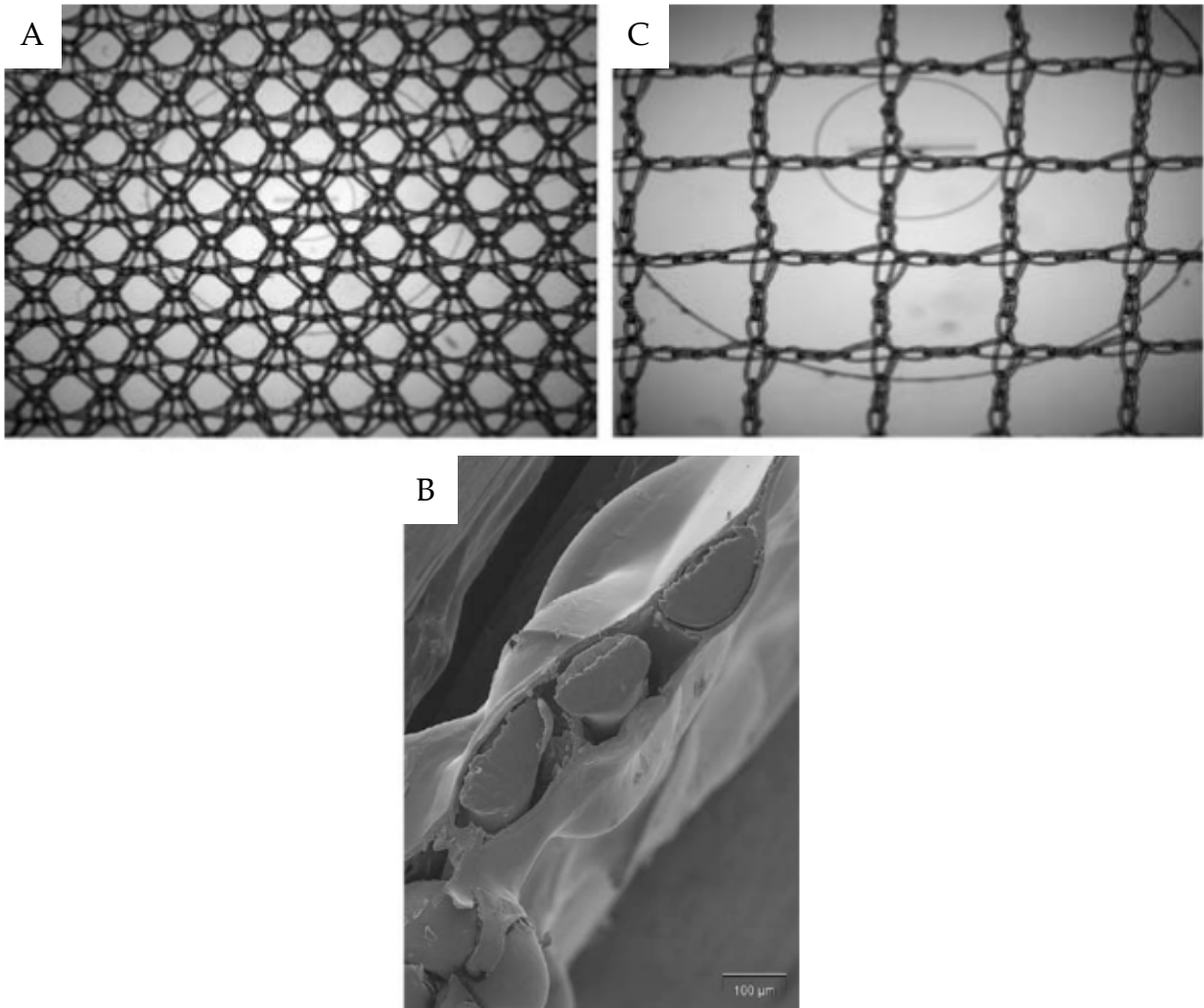


FIGURE 1.4 Macroscopic analysis of commercially available mesh (A) Synthetic: Pelvitex™ (C.R. Bard, Covington, GA, USA) is marketed with a hydrophilic porcine collagen I coat atop polypropylene (28)(B) cross-section of Pelvitex™ under SEM (29); (C) Mixed-type mesh: Popmesh™ (Caldera, Agoura Hills, CA, USA) is manufactured as an ultra-light-weight (19 g/m²) polypropylene material (28)

1.3.2 Surgical Procedures for Pelvic Organ Prolapse (POP)

There are several types of prolapse. Prolapse can affect the vaginal walls, or it can be of one of the pelvic organs: uterine prolapse, enterocele (prolapse of the bowels), cystocele (prolapse of the bladder), or rectocele (rectal bulging caused by wall weakness).

For surgery with prolapse of the bladder, urethra, rectum, and small bowel, the surgeon makes an incision in the wall of the vagina and pulls together the damaged tissue in the area of the prolapsed organ and strengthens the wall of the vagina to prevent recurrent prolapse. For prolapse of the vaginal vault, an incision is made in the wall of the vagina and attaches the top of the vagina to the wall of the lower abdomen, to the spine in the lower back, or to the ligaments of the pelvis (see Fig 1.5).

Surgery can be undertaken choosing either an abdominal or vaginal route. Although precise estimates of the proportion of procedures undertaken by each route are not available, many have suggested that the preferred route for most prolapse surgery is vaginal, with as many as 80–90% of operations done this way (18,30,31).

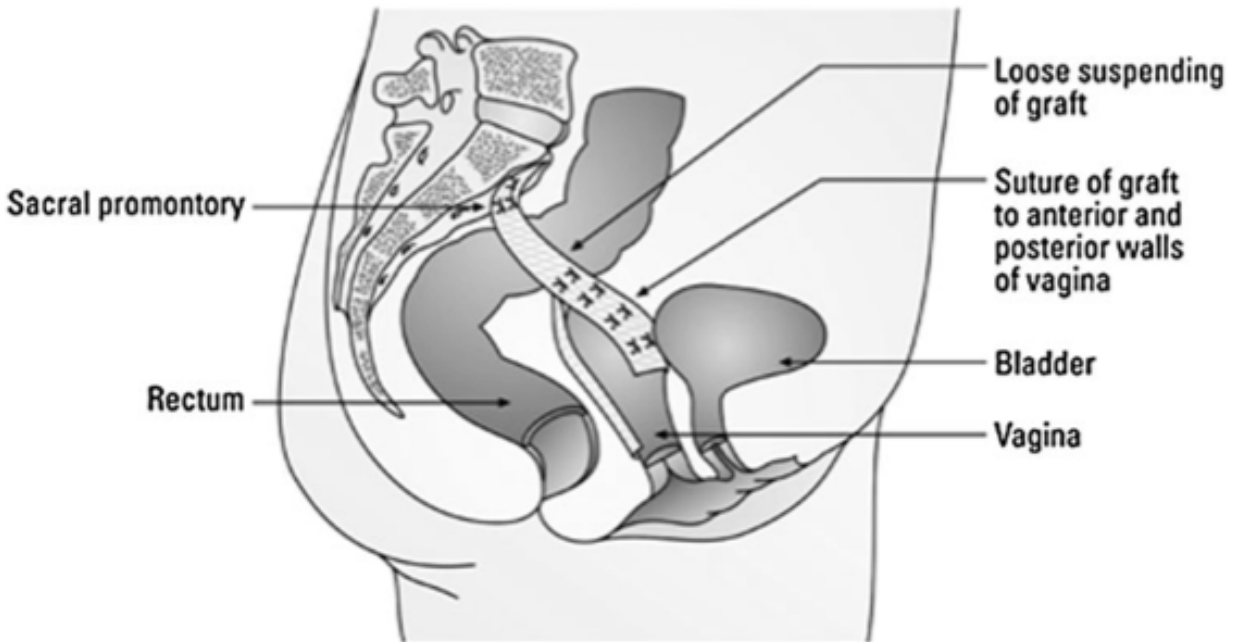


FIGURE 1.5. Polypropylene mesh is placed over the anterior and posterior vaginal walls and then sutured to the anterior sacrum.

1.4 Complications with Urogynecologic Surgical Mesh

Since 11% of American women will require a primary operation for a pelvic organ prolapse (POP) by the age of 80 and almost a third of these women need a second surgery due to recurrence of prolapse and associated complications, urogynecologic mesh has received a lot of attention in recent years (18). Mesh use in POP has rapidly increased in recent years due to the high recurrence rate after native tissue repair. However, complications and recurrence of prolapse are still commonly observed with mesh implantation, especially with the transvaginal approach (32,33). Complications resulting from mesh implantation include shrinkage, erosion, exposure, dyspareunia, discomfort, the inability to walk, and inguinal and gluteal pain. Such complications are significant enough that both USA's Food and Drug Administration (FDA) and UK's

National Institute for Health and Clinical Excellence (NICE) have issued multiple warnings regarding the use of synthetic mesh in vaginal surgery for pelvic floor reconstruction (24,34,35).

Despite its prevalent usage, urogynecologic meshes have had little regulatory oversight. Federal laws have mandated that meshes used in pelvic surgery are not subject to the lengthy and more thorough pre-market approval and are instead considered 510 (k) devices due to the fact there is a predicate, i.e., a device that is based on a similar device that was in use prior to 1976—in this case, hernia meshes (36).

1.5 Evaluating Urogynecologic Mesh on the Market

Most of the scientific work in the field of mesh for pelvic floor repair or hernia repair has been directed towards clinical outcome, especially recurrence rate, bio integration, tissue compatibility, and surgical technique (27,37–42), with the majority focusing on microscopic tissue reaction. Although host response is clearly an important consideration, any variance between the biomechanical properties of implant and surrounding tissue is likely to influence the likelihood of erosion. In recent years, there has been a push to understand more of the biomechanical features of the abdominal wall itself, with the first study being published in 2003.

1.5.1 Evaluation of Biomechanical Properties

The main function of surgical mesh is to provide reinforced support to the damaged tissues with mechanical strength similar to the undamaged native tissue (43–45). Thus, they are a direct reflection of the composition and microstructural arrangement of a tissue, i.e. they provide quantitative information about the tissue

quality. Just as there are many different approaches to determine the structural properties of a complex of tissues, there are also many testing methodologies that can be used to determine the mechanical properties of a specific tissue (3). Tests include uniaxial tensile testing, suture pull-through strength, burst strength, and tear resistance (46). Uniaxial tensile testing, whether cyclical or not, has been the most commonly used tool to compare mechanical properties of urogynecological mesh (3,47).

1.5.2 Histological Outcomes

A multitude of studies have evaluated histology after implantation of scaffolds and mesh materials (39,42,44,48–57). De Tayrac *et al.* looked at collagen-coated vs. non-coated low-weight polypropylene meshes in a sheep model for vaginal surgery (29). Post-implantation results showed that there were no differences observed between the two meshes in terms of shrinkage, tissue ingrowth, inflammatory response, and position of the mesh in the vaginal wall. In vivo studies have shown that polypropylene coated with natural polymers exhibits better tissue incorporation within the pores, less mesh contraction (40,58), and reduced the risk of vaginal erosions (41,59,60). However, none of the coatings have shown improved integration with the surrounding native tissue, i.e., muscle (61–63). Currently, a mesh that, when implanted, allows for muscle tissue ingrowth, contractility, and matches the mechanical integrity of native tissues without significant granulation tissue and or fibrosis remains an area of significant clinical interest.

1.6 Re-establishing Muscle Contractility

While the reason for complications is unknown, most researchers hypothesize that one factor contributing to failure is stiffness. While stiffness means increased tensile strength, it occurs at the expense of tissue function with accelerated tissue contraction, decreased elasticity and compliance, and deterioration of smooth muscle function. After implantation of mesh, substantial fibrosis and little to no smooth muscle ingrowth are commonly observed around the vagina wall.

Therefore, there is incentive to reduce aspects of the foreign body response and improve upon tissue integration after insertion of mesh (64). Previous research conducted on ventral hernia repair indicated that biomaterials have the ability to reduce fibrosis and improve native tissue integration. With native tissue ingrowth into the mesh, a re-establishment of the contractility of the smooth muscle will be possible. The science based approach to evaluation and modulation of the host tissue response to the chitosan coating and the PP mesh has the potential to significantly affect the design of next generation mesh materials and improve outcomes in pelvic floor repair.

1.7 Introduction to Chitosan

It is widely believed that the ideal scaffold material for pelvic floor repair should be one that closely mimics the extra-cellular matrix (ECM), promotes muscle growth, and inhibits fibrosis. In biological organisms, the substrate for most cells is the ECM (65). The ECM adheres to cells with integrins, which are membrane-spanning heterodimeric receptors. Through this adhesion, the ECM regulates cell growth, cell

proliferation, cell differentiation, and matrix remodeling to the cells (65).

There has been a shift towards coating polypropylene mesh with biological materials such as collagen, alginate, and fibrin in recent years(66–68). The mesh and biofilm composite provides a polypropylene skeleton for mechanical support with a biofilm that is believed to minimize both inflammatory response and fibrosis. However, reviews have been a mixed response with heavy lot-to-lot variation and difficulty controlling the mechanical properties of the neo-tissue after implantation of mesh. Chitosan-based biomaterials may be ideal candidates for use in coating surgical mesh materials. In addition to being inexpensive and easy to handle, the physical properties of chitosan can be altered by changing the deacetylation percentage and molecular weight. Chitosan is produced commercially by deacetylation and depolymerization of chitin, which is a structural polymer that makes up the exoskeleton of crustaceans. It is composed of poly-N-acetylglucosamine units bound by β -1, 4 glycosidic bonds as a linear polymer of 2000-3000 units (69).. The most prevalent chitosan used for biomaterial applications is 85% deacetylated with 600,000-800,000 molecular weight.

Mechanistically, addition of chitosan, may provide much more amino groups for cell adhesion and proliferation due to the affinity between positively charged ammonium groups of chitosan and negatively charged cell membrane surfaces (70). Muzzarelli *et al.* found that chitosan stimulates wound healing and increases angiogenesis; due to integrin engagement and improved expression of cytokines and growth factors. This has broad implications in a clinical context but also as a tool to distinguish the molecular mechanisms regarding cell–cell and cell–matrix interactions in the course of wound healing (71).

The polysaccharide chitosan has been found to be a effective material in a broad

spectrum of applications due to its unique biological properties including nontoxicity, affinity for protein adsorption, antibacterial, fungistatic, and anti-tumoral properties (72). When applied to dermal wounds, chitosan was observed to decrease fibroblast infiltration and fibrosis (73), eliciting a more "constructive" response rather than the typical fibroplasia type response observed upon implantation of synthetic materials (69). Other studies have shown that chitosan can serve as a construct for smooth muscle ingrowth, but further work is needed to understand chitosan's effect on muscle contractility, matching mechanical properties of native tissue, and inflammatory response (74).

Additionally, chitosan can be formed as interconnected-porous structures by freezing and lyophilization of chitosan solutions. The porous nature of the resulting chitosan scaffold is desirable because it allows for cells migrate and proliferation not only on the surface, but also within the bulk of the material (72). Creating a three-dimensional inter-connected pore architectures at the microscale level has been shown in multiple applications to reduce the typical fibroplasia observed following the implantation of a number of common synthetic polymers (75).

1.8 Overview and Study Objectives

The objective of this research was to establish the effects of chitosan on polypropylenes mesh both *in vitro* and *in vivo*. First, we looked at attachment of fibroblasts and myoblasts on chitosan-coated polypropylene mesh and polypropylene mesh *in vitro*. We developed various concentrations of chitosan coatings and were able to characterize the mesh samples using Fourier transform infrared spectroscopy. We harvested myoblasts and fibroblasts from neonatal mice and seeded them 1:1 atop the

mesh samples and analyzed the cell growth and ratio of cell types. Second, we took the mesh samples and implanted them in a rat abdominal wall model and looked a variety of different metrics: tetanic force generation, histological assessment, myogenin expression, macrophage typing, mechanical strength, and the collagen I/III content and ratio. The following specific aims were examined:

1.8.1 Objective I

Specific aim 1 (Chapter 2): To measure cell attachment of a co-culture of myoblasts (myo) and fibroblasts (fb) on mesh samples developed for muscle tissue ingrowth.

In this study, we hypothesized that coating polypropylene mesh with chitosan will preferentially enhance the attachment of myoblasts in co-culture with fibroblasts. We found that application of a 0.5% (w/v) chitosan-coated polypropylene elicited preferential attachment of myoblasts over fibroblast attachment *in vitro*. This was the first study of its kind to use the ratio of myoblasts to fibroblasts as a metric for evaluation. This study makes up the first half of Chapter 2.

1.8.2 Objective II

Specific aim 2 (Chapter 2): Determine if chitosan encourages functional muscle growth and lessens typical fibroplasia observed following the implantation of polypropylene *in vivo*.

We hypothesized that chitosan-coated polypropylene mesh will promote muscle tissue

ingrowth and decrease inflammatory response in a rat abdominal wall model. We found that chitosan-coated polypropylene mesh promotes tissue ingrowth:

- Functional muscle testing show 0.5% chitosan-coated polypropylene mesh generates significantly higher tetanic force than polypropylene mesh
- Neo-tissue surrounding Ch-PPM was characterized by myogenin expression between mesh fibers as opposed to polypropylene and collagen-polypropylene mesh samples

Additionally, chitosan-coated polypropylene mesh induced moderate inflammatory response:

- Histology showed narrow band of fibrosis, high number of macrophages
- Characterized by early presence of macrophages (Type M2) that have been shown to lead to better remodeling outcomes

This study makes up the second half of Chapter 2.

1.8.3 Objective III

Specific Aim (Chapter 3): Examine the neo-tissue surrounding three different mesh samples to evaluate muscle tissue strength and collagen incorporation in a rat abdominal wall model.

We hypothesized that a reduction in the ratio of collagen types I/III of the neo-tissue results in a structurally weaker tissue. The results of this study indicate that there is no significant difference in the ratio of collagen type I/III based on area or the absolute quantity of collagen types in mesh samples at either 4 weeks or 12 weeks. We do not

believe there is a relationship between the amount of collagen I/III ratio and mechanical strength in our samples, rather mechanical strength could be dependent on the cross-linking and structure of collagen fibers. This study is described in Chapter 3.

Chapter 2

Measuring the attachment of myoblasts on chitosan-coated vs. non-coated polypropylene mesh in vitro¹

2.1 Introduction

Use of a knitted mesh is a common method indicated for mechanical reinforcement for abdominal hernia reconstruction and pelvic organ prolapse repair (1). Recurrence of ventral hernias after open suture repair can occur with a reported frequency of 31-49% when performed without mechanical reinforcement provided by the mesh (37). At least 29% of those that opt for surgery of pelvic organ prolapse and incontinence will require re-operation (18). When used as a mechanical reinforcement in functional muscle repair, a synthetic mesh is intended to serve as a permanent implant, which remains in the patient for life (34,38). Synthetic mesh, such as polypropylene mesh, is widely used due to its high strength. However, although the use of synthetic mesh materials significantly reduces recurrence rates by providing strong mechanical

-
1. ¹ Udpa N., Iyer S.R., Rajoria R., Breyer K.E., Valentine H., Singh B., McDonough S.P., Brown B.N., Bonassar L.J., Gao Y. "Effects of chitosan coatings on polypropylene mesh for implantation in a rat abdominal wall model", Tissue Engineering. Accepted.
DOI: <http://online.liebertpub.com/doi/pdf/10.1089/ten.tea.2012.0739>

support to abdominal wall or pelvic floor, commonly used synthetic polymers can sometimes elicit a strong foreign body reaction, often resulting in fibrous tissue encapsulation, erosion, or mesh degradation with high infection rates (76,77). These common outcomes following mesh implantation can result in discomfort for the patient and, in some cases, a need for revision or removal of the implant. The complications are significant enough that FDA issued warnings in 2007 and 2011 regarding the use of polypropylene mesh on the pelvic floor.

Therefore, there is incentive to reduce aspects of the foreign body response, characterize macrophage phenotype, and improve upon tissue integration after insertion of mesh (56,64,78). An ideal mesh for use in abdominal hernia repair and pelvic floor reconstruction would provide strength and elasticity similar to native tissues, i.e., muscle tissue, as well as elicit tissue incorporation in place of fibrous tissue ingrowth and be resistant to infection (60,79,80). Progressive ingrowth of fibrous tissue inhibits the integration of the implanted material within the tissue of interest and leads to a mismatch in mechanical properties with native tissue. Ideally, the mechanical properties of the neo-tissue should be strong enough to prevent recurrence, but not so strong as to reduce compliance of the abdominal wall or the vaginal tissue and cause adhesion formation or unpredicted mesh shrinkage (44). This often results in pain or discomfort, which may require corrective surgeries due to complications including mesh erosion and mesh exposure. Materials, which preferentially promote the attachment of myoblasts over fibroblasts, may elicit a less fibrotic host tissue response *in vivo*.

Chitosan-based biomaterials may be ideal candidates for use in coating hernia and pelvic floor mesh materials. The polysaccharide chitosan has been shown to be an

effective biomaterial in a broad spectrum of applications due to its unique biological properties including nontoxicity, affinity for protein adsorption, antibacterial, hemostatic, fungistatic, and anti-tumoral properties (72). Additionally, the physical and chemical properties of chitosan can be tailored to specific applications by relatively simple alterations the molecular weight and deacetylation percentage (72). Previous work has highlighted mechanical properties (57,81) or inflammatory response (38,81–83) of chitosan-based materials in abdominal wall models of small animals, however there is no report describing the effect of chitosan-coated mesh on functional muscle tissue ingrowth. Given that hernia is induced by damages to the abdominal wall skeletal muscle, inflammatory response and tissue rebuilding to implantation of surgical mesh should include skeletal muscle ingrowth. We believe that by analyzing the skeletal muscle functionality, i.e., active muscle force generation, data that is more physiologically relevant for repair can be provided.

The objective of our study is to examine the effects of chitosan coatings on polypropylene mesh. We hypothesized that the chitosan coating will promote muscle tissue ingrowth and decrease the inflammatory response. Both *in vitro* and *in vivo* studies were conducted to test this hypothesis. In the *in vitro* study, 1:1 co-culture of myoblasts and fibroblasts showed preferential attachment of myoblasts over fibroblasts to chitosan-coated polypropylene mesh. The *in vivo* study was performed in an established rat model of abdominal wall defect repair (63). The functional muscle response, histologic response and macrophage phenotype of the reconstructed tissues were examined at 2, 4, and 12 weeks post-implantation.

2.2 Materials and Methods

2.2.1 Overview of Experimental Design

All procedures were performed in accordance with the National Institute of Health (NIH) guidelines for care and use of laboratory animals, and with approval of the Institutional Animal Care and Use Committee (IACUC) at Cornell University. The study involves both *in vitro* and *in vivo* experiments. The *in vitro* study was performed using a reference polypropylene mesh (Avaulta Solo®, C.R. Bard) and different concentrations of chitosan coatings on polypropylene mesh. The mesh coated with chitosan that maximized cell attachment and yielded a high myoblast to fibroblast ingrowth ratio was selected for the *in vivo* study. In the *in vivo* portion of the study, an additional mesh was added, a monofilament polypropylene mesh coated with hydrophilic porcine collagen (Pelvitex™, C.R. Bard Inc., Covington, GA, USA).

2.2.2 Preparation of Chitosan-coated Meshes and Characterization

High molecular weight chitosan, >75% deacetylated, ~600,000 MW (Sigma Aldrich, Milwaukee, WI) was added to distilled H₂O at concentrations of 0.3%, 0.5%, and 0.7% (w/v) and 1% (v/v) acetic acid solution until a clear solution was obtained. The sterile PPM was cut into 1.2 x 1.2cm squares and placed into a sterile bottle containing the 0.2µm-filtered chitosan-solution and stir bar. The mesh was removed from the solution, placed in a centrifuge tube, and left in liquid nitrogen for several hours while being placed in the lyophilizer at -40°C for 24 hours. Mesh were sterilized under ultraviolet light for 20 minutes. Scanning electron microscope (Leica 440, Buffalo Grove, IL) and Fourier transformation infrared spectroscopy (Bruker Vertex 80v,

Billerica, MA) using Opus 6.0 Software was used to confirm the successful coating. PPM was also subjected to the same coating procedure minus the addition of chitosan to ensure that procedural effects do not alter the structure of the PPM material. Pore diameters were measured from the SEM images using ImageJ 1.45s (NIH, 2009). A representative mesh of each Ch-coated mesh type was selected, imaged, and 10 chitosan pores were selected at random for measurement. The range was recorded.

2.2.3 Overview of in vitro Study

Neonatal and adult CD-1 mice (Charles River Laboratories International, Inc., Wilmington, MA) were sacrificed for isolation of myoblasts and dermal fibroblasts, respectively. Isolation of cell types was modified from pre-existing protocol (84). Cells were independently passaged to four generations, stained with a long-term lipophilic tracer and then seeded 1:1 atop one of four different test articles: polypropylene mesh (PPM), 0.3% Chitosan coated PPM (Ch-PPM), 0.5% Ch-PPM, and 0.7% Ch-PPM. The mesh samples were imaged at 12 hours, 24 hours, and 48 hours.

2.2.4 In vitro Immunocytochemistry & Co-culture

Isolation of myoblasts and fibroblasts from mice and appropriate cell culture mediums were adapted from pre-existing protocol (84). At Passage 4, a sample of myoblasts and a sample of fibroblasts were seeded separately on glass slides and prepped for immunocytochemistry. All staining procedures were followed according to vendor instructions (Abcam, Cambridge, MA). After a DAPI stain, the primary antibodies used for antibody labeling were [1] rabbit polyclonal anti-desmin (Abcam) at

1:80 dilution for identification of myoblasts, and [2] rabbit polyclonal anti-fibroblast-specific-protein-1 (Abcam) at 1:40 dilution for identification of fibroblasts. The secondary antibodies used were [1] goat polyclonal secondary antibody to rabbit (FITC) at dilution 1:1000, and [2] goat polyclonal secondary antibody to mouse (TRITC) at dilution 1:1000, respectively. Plates were viewed with an inverted microscope (Olympus IX-71, Tokyo, Japan), and images were recorded using CellSens software. The images were overlaid, and the numbers of Desmin⁺/DAPI⁺ and FSP1⁺/DAPI⁺ cells were determined in four random quadrants per dish. If cells were determined to be >95% pure, the cells remaining in culture were stained with long-chain carbocyanines: fibroblasts were stained with DiI (Invitrogen) and myoblasts were stained with DiO (Invitrogen) following instructions provided by the vendor. Following determination of purity of the desired cell culture, myoblasts and fibroblasts were seeded onto the 1.2 x 1.2 cm mesh samples at a cell density of 2.4×10^5 cells/cm². To increase wettability, all mesh samples were soaked in media for 1 hour prior to cell seeding.

2.2.5 In vitro Characterization of Cell Attachment on Mesh

An IX-71 Olympus microscope was used to determine the ratio of the area and number of myoblasts and fibroblasts at 12, 24, and 48 hours. To image the mesh, 40x magnification was used. Each mesh was analyzed for cell numbers and cell area. The location chosen for imaging remained consistent amongst all mesh samples (identical weave pattern). Images were captured highlighting the fluorescent markers for myoblasts and fibroblasts, and cell area was determined by dividing the number of fluorescent pixels by the total number of pixels in the digital image. Total numbers of

each cell type were evaluated using ImageJ 1.45s (NIH, 2009). To confirm that chitosan remained on coated mesh samples for the duration of the *in vitro* study FTIR analysis was conducted again after 48 hours of the mesh being submerged in media.

2.2.6 Overview of in vivo Study

Male Wistar rats (Charles River Laboratories International, Inc.) between 250-450 grams were randomly assigned to nine groups of six each. Each rat was subjected to a partial thickness excision of a 1.2 cm x 1.2 cm section of the ventrolateral abdominal wall musculature on either side of the linea alba. The defects were repaired with one of three test articles: Ch-PPM, collagen coated-PPM, or Col-PPM (Pelvitex™), and PPM alone. The animals were randomly divided into 3 groups after surgery for survival of 2, 4, and 12 weeks. The harvested tissues were evenly split for measurement of active muscle force by contractile test, histological analysis, and macrophage phenotyping. Native tissue was also tested as a baseline control.

2.2.7 In vivo Surgical Procedure

Each rat was placed in a transparent plastic anesthesia induction chamber to administer inhalation anesthesia with 2.5% isoflurane and an oxygen flow rate of 1 L/min. The ventral abdomen was clipped from the xiphoid process to the pubis, and sterile prepped with povidone-iodine scrub and warm saline. The animal was then transferred to the surgical table with a sterile drape applied over the ventral abdomen for a surgical procedure adapted from a well-established model (63). A 4cm ventral midline abdominal skin incision was made, and the skin and subcutaneous tissue were

separated from the underlying musculature. Bilaterally, a 1.2 cm x 1.2 cm section of the external and internal abdominal oblique layers of the ventrolateral abdominal wall was excised while the underlying transverse abdominus and peritoneum remained intact. Different test articles were placed in the ventrolateral defects and oriented with the weave pattern perpendicular to the linea alba. The defect was repaired with a size-matched piece of the chosen test article that was randomly selected prior to surgery. PROLENE™ sutures (Ethicon Inc., Somerville, NJ) were placed at each of the four corners of the test article to secure the mesh to the surrounding musculature. A MONOCRYL™ suture (Ethicon Inc.) was used to close the skin incision. Each animal was recovered from anesthesia and returned to the housing unit. Each rat received meloxicam by subcutaneous injection on the day of surgery and for two additional days. The general health status and surgical site were monitored daily and recorded for the duration of the study.

2.2.8 In situ Force Generation Testing

Force generation tests were included to evaluate functional muscle tissue ingrowth in neo-tissue. In the first group, the rats were anesthetized by isoflurane 2, 4 or 12 weeks after insertion of surgical mesh, and placed on an in-situ mounting apparatus. The skin and the underlying connective tissue were cleared from the surgical mesh placement site. The four visible PROLENE™ sutures, previously used to attach the surgical mesh to the partial defect, identified surgical mesh placement site. The tests to determine the contractile property of the tissue were adapted from the protocol previously described by Valentin, *et al* (2010), using a muscle testing system (Aurora

Scientific Inc., Toronto, Canada).

After creating a tissue flap, in order to perform the testing across the muscle sections uniformly, the resting tension was set at approximately 2g before testing. The tetanic force was generated at this length with electrical stimulation for one second at frequencies of 30, 60, 70, and 80 Hz with a rest period of two minutes following each tetanic force generation. The maximum tetanic force generation for each frequency was recorded by averaging the tetanic force generation of the muscle from 0.1 second after start of stimulation to 0.1 second before end of stimulation, subtracted by the resting tension.

2.2.9 Histology

In the second group, after rats were euthanized, constructs were dissected off and split into two sets, for I) H&E staining and II) macrophage phenotyping and myogenin expression. The first set was fixed by immersion in 10% neutral buffered formalin, embedded in glycol methacrylate (GMA), sectioned at 3 μ m and stained with hematoxylin and eosin (H&E). A board certified veterinary pathologist (SPM), who was blinded to the treatment groups, examined the H&E stained mesh constructs by light microscopy. The severity of the inflammatory response was assessed using a well established grading scheme (Table 2.1) with minor modifications (85,86): the width of the inflammatory reaction and scar were measured on a digital image of each slide created with an Aperio ScanScope microscope slide scanner (Carlsbad, CA). The ruler tool in the Aperio ImageScope v9.1.19 software was calibrated using a digital image of a 1 mm calibration slide (Carl Zeiss, Oberkochen, Germany). The average width of the

inflammatory reaction or scar obtained from a total of 10 sections selected at random along the length of the construct was used in the tissue reaction-scoring scheme. Each sample received a scoring outcome of mild, moderate, or severe inflammatory response.

TABLE 2.1. Method of semi-quantitative histopathological assessment

1. Tissue reaction scoring

Tissue Reaction Element	Grading Factor x Weight Factor = score	
Width of inflammation ^a	5	=
Width of scar ^a	1	=
Overall density of cellular reaction ^b	5	=
Number of cells ^a		
Neutrophils	6	=
Lymphocytes	2	=
Plasma cells	2	=
Eosinophils	1	=
Macrophages	1	=
Giant cells	1	=
Fibroblasts	1	=
TOTAL SCORE		

2. Tissue reaction grade

Total Score	Tissue Reaction Grade	Designation
1-10	1	Minimal
11-25	2	Mild
26-40	3	Moderate
>40	4	Severe

a.	Width of Inflammation or Scar (diameter of response in um)	No. Cells (per 60x field)	Grade
	0	0	0
	1-200	1-50	1
	201-400	51-100	2
	401-600	101-200	3
	>600	>200	4

b. Overall Density of Cellular Reaction (assignment based on experience of pathologist)

Bare scattering	1
	2
	3
Dense aggregation	4

2.2.10 Assessment of Macrophage Phenotype and Expression of Myogenin

Macrophages have been described to have a spectrum of phenotypes, which range from classically activated and pro-inflammatory (M1) to alternatively activated, anti-inflammatory, regulatory and wound healing (M2). Using the second set of the mesh used for histology purposes, the phenotype of macrophages responding to each mesh material were assessed as previously described (56) after embedding in paraffin. Briefly, histologic sections were de-waxed through immersion in xylenes and a graded series of ethanol (100-70%). Antigen retrieval was then performed by immersion in 10 mM citric acid monohydrate (pH 6.0) at 95°C for 20 minutes. The slides were allowed to cool and were then washed in TRIS buffered saline / Tween 20 solution (pH 7.4) and PBS. The sections were then blocked in 2% normal horse serum, 1% BSA, 0.1% Triton X-100, and 0.1% Tween 20 in PBS (pH 7.4) for 1 hour at room temperature. The sections were then exposed to antibodies specific for a pan-macrophage (M0) marker (1:50; mouse anti-CD68; Serotec), a M1 phenotype marker (1:50; rabbit anti-CD86; Abcam), and an M2 phenotype marker (1:50, goat anti-CD206; Santa Cruz) overnight at 4°C. The slides were washed in PBS and then incubated in appropriate secondary antibodies. The secondary antibodies used were Alexa Fluor donkey anti-mouse IgG (594 nm; 1:150; Life Technologies), Alexa Fluor donkey anti-goat IgG (488 nm; 1:150; Life Technologies) and donkey anti-rabbit IgG PerCP 5.5 (1:200; Santa Cruz). The slides were then cover-slipped with aqueous mounting media containing DAPI. Representative sections from each sample group at the 14-day time point were examined and imaged by a blinded investigator using a Nikon e600 microscope equipped with a Nuance multi-spectral imaging system.

Myogenin is a part of the myogenic regulatory gene family, which includes MyoD, myf5 and MRF4. These genes encode a set of transcription factors that are essential for muscle development. Expression of myogenin is limited to cells of skeletal muscle origin(87). Additional sections were taken from the paraffin embedded blocks used for macrophage phenotype. These sections were stained with monoclonal mouse anti-myogenin clone F5D (Dako North America, Inc., Carpinteria, CA). All staining procedures were followed according to vendor instructions. Representative sections from each sample group were imaged at the 14-day time point.

2.2.11 Statistical Analysis

For *in vitro* results in Figure 2.3a, statistical significance ($p < 0.01$) was calculated using a two-way ANOVA with mesh, time, and their interaction term as independent variables. Statistical significance ($p < 0.01$) was calculated using a two-way ANOVA with mesh and time and their interaction term as independent variables. The interaction term was significant [$F(6,24) = 21.67, n=3, p < 0.001$]. Differences between mesh samples at different time points were analyzed using a Tukey's HSD post-hoc comparison (JMP, v.9). All values are expressed as the least mean square mean \pm standard deviation.

For Figure 2.3b, statistical significance ($p < 0.05$) was calculated using a two-way ANOVA with mesh and time and their interaction term as independent variables. Differences between mesh samples at different time points were analyzed using Tukey's HSD post-hoc comparison. The analysis was done on a log-transformed dependent variable. The interaction term was significant [$F(3,16) = 23.36, p=0.0027$]. Differences between mesh samples at different time points were analyzed using a Tukey's HSD post-hoc comparison with a Bonferroni correction for multiple

comparisons. All values are expressed as the least mean square mean \pm standard deviation.

For *in vivo* results, in Figure 2.4, data was analyzed with JMP using a mixed model with random effect being the rat ID and the fixed effects being the mesh type. Both time and the interaction term of time and mesh type were independent variables. Statistical analysis was done using a mixed model with Tukey's HSD post-hoc comparison ($n = 4$, $p < 0.05$). Dashed line denotes force generation of native muscle tissue. All values are expressed as the least mean square mean \pm standard error.

2.3 Results

2.3.1 Analysis of Mesh Materials by SEM and Fourier Transformation Infrared Spectroscopy (FTIR)

Figure 2.1 shows the microarchitecture of the mesh materials as observed under SEM. The polysaccharide was distributed within the interstices of the mesh fibers for the Ch-PPM samples. The chitosan microarchitecture differed between 0.3%, 0.5% and 0.7% Ch-PPM. The chitosan pore size of the different mesh samples varied. PPM has mesh pore sizes that measured 2.0×1.7 mm, the 0.3%, 0.5%, and 0.7% Ch-PPM has chitosan pore diameters within the polypropylene interstices that ranged from $200\mu\text{m}$ - 1.7mm , $80\mu\text{m}$ - $140\mu\text{m}$, and $10\mu\text{m}$ - $60\mu\text{m}$, respectively.

As seen in Figure 2.2, the PPM exhibits peaks at 1375 cm^{-1} and 1450 cm^{-1} representing the alkane groups, and at $2600\text{-}3000\text{ cm}^{-1}$ representing the methylene and methyl groups. FTIR spectra of the Ch-PPM samples depict characteristic absorption

bands at 1089 cm^{-1} , $1600\text{-}1750\text{ cm}^{-1}$, and 3370 cm^{-1} , which represent glycosidic bonds, residual carbonyl groups, and the stretching vibration of the NH_2 and OH groups, respectively. These peaks were seen to increase with increasing chitosan concentrations. The FTIR after 48 hours results showed that: 1) after 48 hours, there is still chitosan attached to the mesh; and 2) the coating procedure does not affect the structure of PPM material. These two observations lead us to believe that the higher myoblast to fibroblast ratio is due to the chitosan coating.

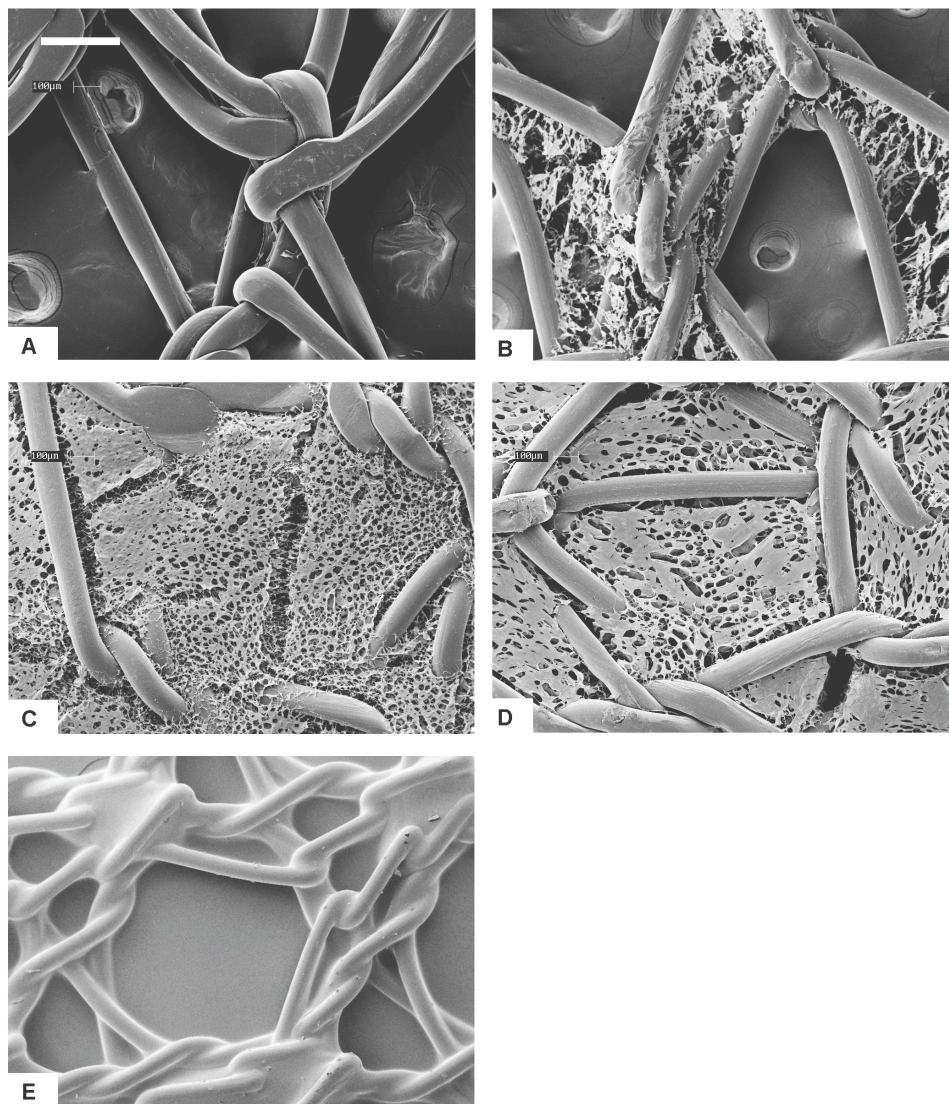


FIGURE 2.1. Scanning electron microscope (SEM) micrographs of mesh types (A) Avaulta Solo® C.R. Bard, knitted polypropylene mesh (PPM), (B) 0.3% Ch-PPM, (C) 0.5% Ch-PPM, (D) 0.7% Ch-PPM, (E) Pelvitex™, C.R. bard, collagen-coated polypropylene mesh (Col-PPM). Scale bar = 100 µm. Ch-PPM, chitosan-coated PPM.

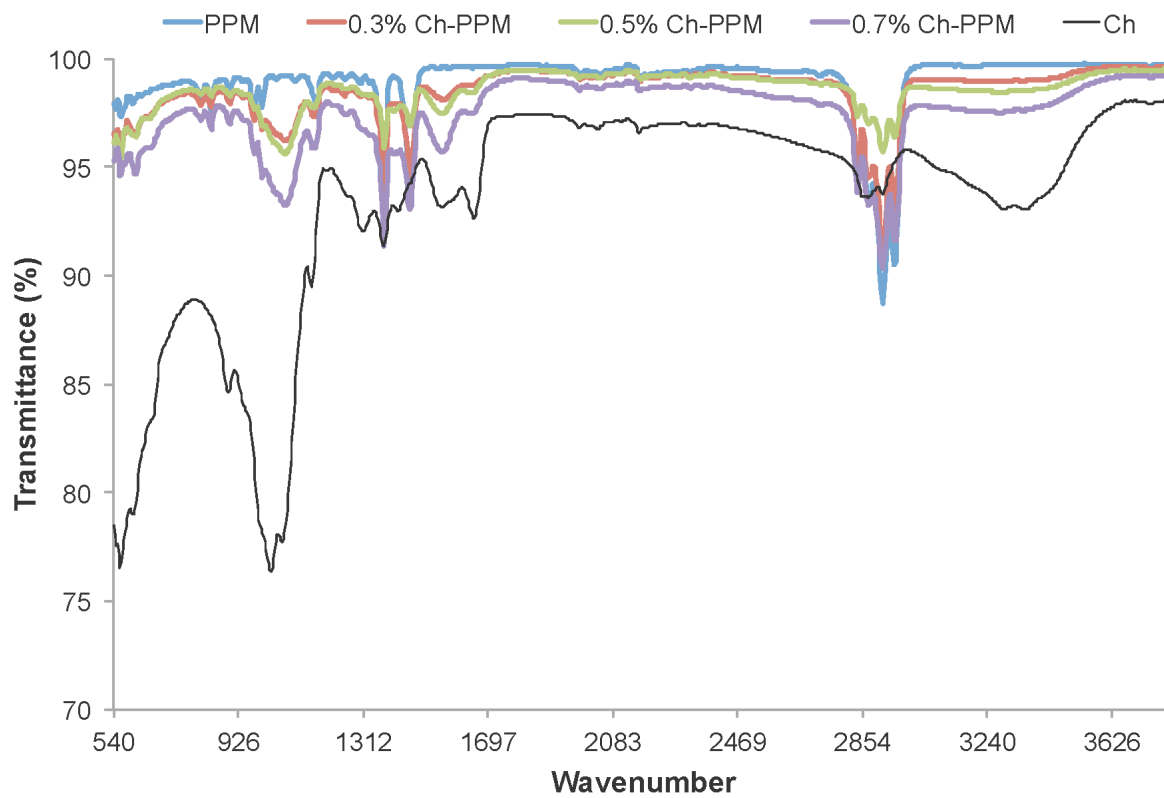


FIGURE 2.2. FTIR spectra of high molecular weight chitosan (600,000 MW) and uncoated PPM, 0.3% Ch-PPM, 0.5% Ch-PPM, 0.7% Ch-PPM. FTIR, Fourier transformation infrared spectroscopy.

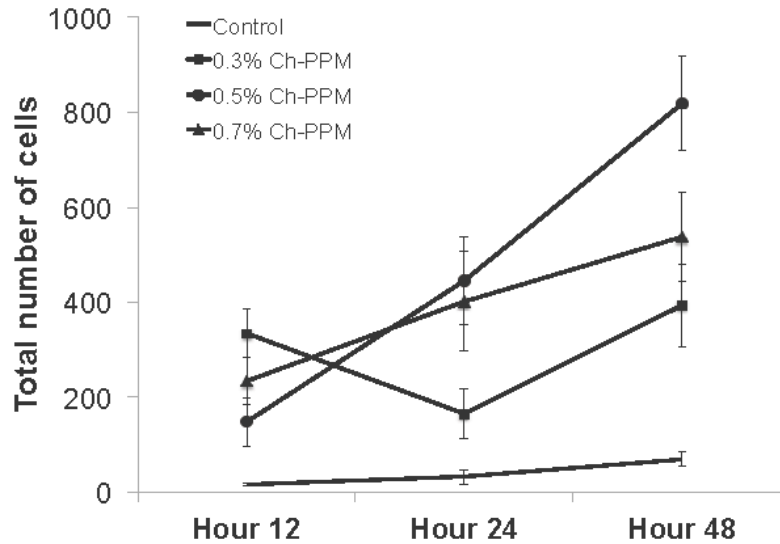
2.3.2 Characterization of Cell Attachment on Mesh using Fluorescent Microscopy

The ratio of myoblasts to fibroblasts on the surface of cell seeded mesh materials was measured using a pixel count of the DiO:DiI, respectively. By day 2, the total number of cells was significantly greater for all three Ch-PPMs than for the reference mesh (Fig. 2.3a). The ratio of myoblasts to fibroblasts for 0.3%, 0.5%, and 0.7% Ch-PPM consistently remained greater than 1 (Fig. 2.3b), indicating a higher number of attached myoblasts in comparison with fibroblasts both within the mesh interstices and atop the polypropylene fibers. The control material had a ratio of less than 1, suggesting more fibroblasts attached than myoblasts.

Statistical analysis of the same mesh across the three different time points was completed to analyze the proliferation of cells from 12 hours to 48 hours. 0.5% Ch-PPM at 48 hours was significantly different from the number of cells that attached to the same mesh at both 12 hours and 24 hours. The number of cells that attached to 0.5% Ch-PPM at 24 hours was significantly different from the cells that attached at 12 hours. 0.5% Ch-PPM was the only mesh to show a significant difference across the three time points. As a result, 0.5% Ch-PPM was selected for the *in vivo* portion of the study.

A)

Statistical Analysis	Hour 12	Hour 24	Hour 48
Control (PPM)			α
0.3% Ch-PPM	* #		*
0.5% Ch-PPM		*+ α	*+ % α β
0.7% Ch-PPM	*	*+ α	* α



B)

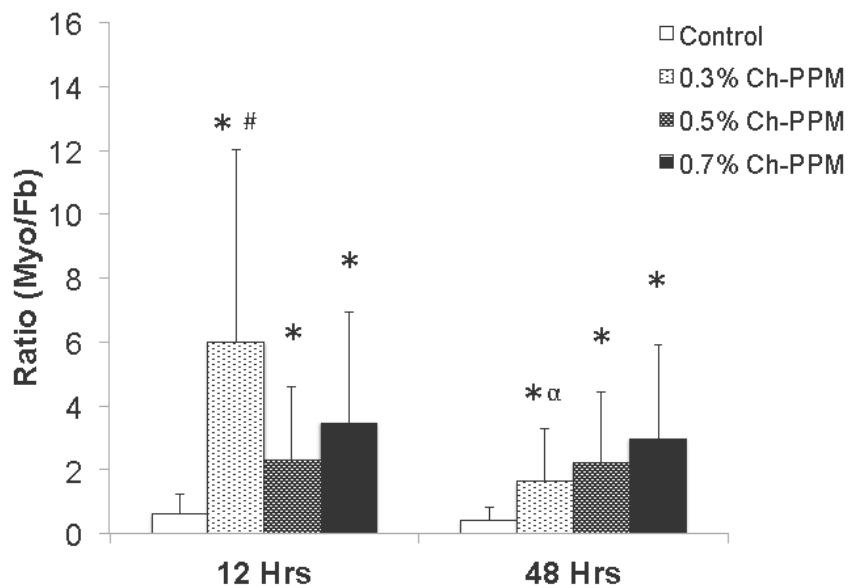


FIGURE 2.3. (A) Total number of cells attached to mesh samples. “*” indicates significantly different from control within time point, “+” indicates significantly different from 0.3% Ch-PPM within time point, “#” indicates significantly different from 0.5% Ch-PPM within time point, “%” indicates significantly different from 0.7% within time point, “a” indicates significantly different from 12-h time point within the same mesh type, and “b” indicates significantly different from 24-h time point within the same mesh type. (B) The ratio of myoblast:fibroblast (myo/fb) for mesh samples. The ratio was measured using the DiO:DiI fluorescence ratio. “*” indicates significantly different from control within time point, “#” indicates significantly different from 0.5% Ch-PPM within time point, and “a” indicates significantly different from 12-h time point within the same mesh type.

2.3.3 Analysis of Force Generation

No significant differences were present amongst the different meshes after 2 weeks and 4 weeks of implantation (Fig. 2.4). After 12 weeks of implantation 0.5% Ch-PPM had significantly higher tetanic force response at stimulation frequency of 60 Hz than PPM. PPM showed negligible contractile response at 12 weeks, while Ch-PPM approached native tissue better than the PPM and in terms of tetanic response at 12 weeks. Furthermore, contractile response of 0.5% Ch-PPM significantly increased between 2 weeks and 12 weeks; whereas there was no significant difference between PPM and Col-PPM.

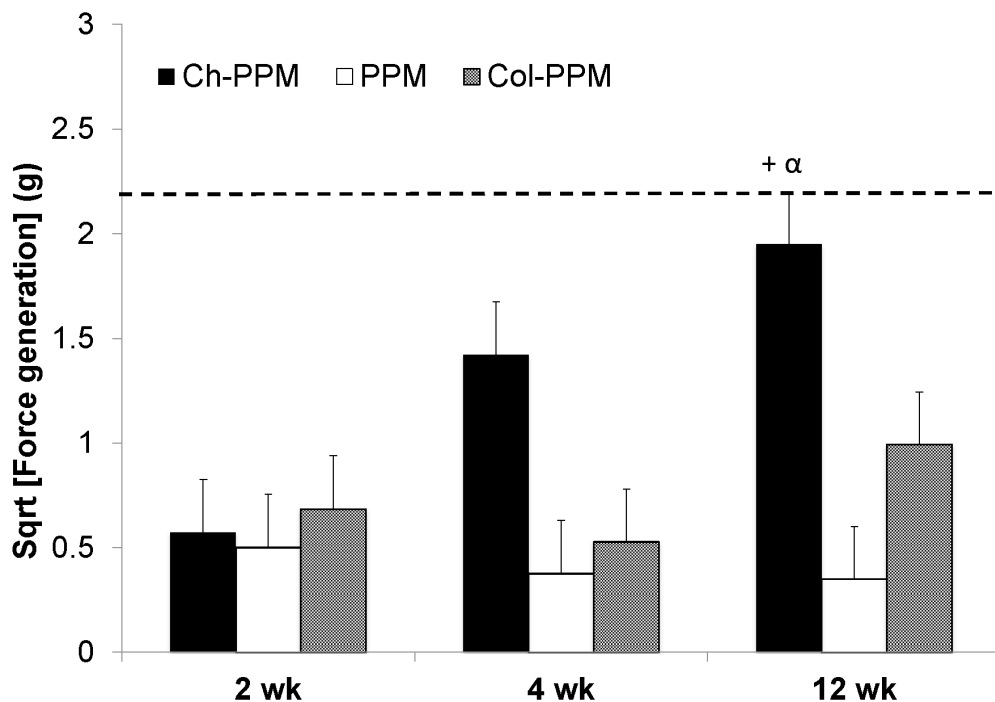


FIGURE 2.4. In situ force generation of mesh samples. Dashed line indicates force generation of native tissue. “+” indicates significantly different from 12-week PPM within time point, “a” indicates significantly different from 2-week Ch-PPM.

2.3.4 Histopathological Assessment

Table 2.2 summarizes the histopathological assessment of the mesh samples after implantation in the abdominal wall. At 2 weeks post implantation, the semi-quantitative histopathological assessment for the degree and type of cellular infiltrate was moderate for all meshes. The tissue reaction score for the Ch-PPM remained unchanged out to 12 weeks. In contrast, the average tissue reaction scores for both the PPM and the Col-PPM increased at 12 weeks. Although the average tissue reaction score for the Ch-PPM (35 ± 3.3) was not statistically significantly different from that of the PPM ($p = 0.08$) or the Col-PPM ($p = 0.09$) a clear trend was evident with a less intense tissue reaction induced by the Ch-PPM (Fig. 2.5a). Strikingly, PPM at 12 weeks, was accompanied by locally extensive areas of dystrophic mineralization (Fig. 2.5b&c). No dystrophic mineralization was detected around any of the Ch-PPM. The PPM was infiltrated by a large population of mixed mononuclear cells (Fig. 2.5b). In contrast, the inflammatory infiltrate around the Col-PPM was similar to that around the Ch-PPM but with a moderately greater fibrotic response (Fig. 2.5c). Figure 2.6 illustrates the stable tissue reaction to the Ch-PPM at 2, 4 and 12 weeks post implantation.

TABLE 2.2 Mean rounded scores, width of inflammatory response, and width of fibrosis for each implant^a

<i>Mesh (weeks)</i>	<i>Average tissue reaction score^b</i>	<i>Average width of inflammatory response [$\mu\text{m} \pm (1 \text{ SD})$]</i>	<i>Average width of fibrotic response [$\mu\text{m} \pm (1 \text{ SD})$]</i>
Ch-PPM			
2	34 (5.0)	657 (323.1)	269 (86.3)
4	32 (11.4)	162 (137.3)	440 (183.2)
12	35 (3.3)	426 (137.9)	122 (40.9)
PPM			
2	33 (0)	575 (36.8)	185 (2.8)
4	31 (7.8)	174 (167.0)	461 (129.1)
12	45 (11.1)	535 (245.9)	235 (179.60)
Col-PPM			
2	43 (10.1)	1150 (1149.5)	1468 (856.5)
4	27 (5.0)	57 (19.9)	272 (104.3)
12	46 (12.5)	549 (181.8)	143 (40.6)

^aScores, width of the inflammatory reaction and the width of the fibrotic response (scar) for each time point were averaged and the mean rounded to obtain the final result (one SD).

^bTissue reaction scores: 0 = normal; 1–10 = minimal; 11–25 = mild; 26–40 = moderate; > 40 = severe.

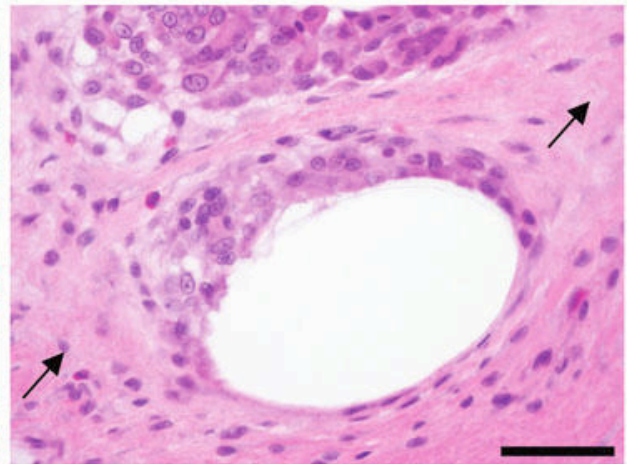
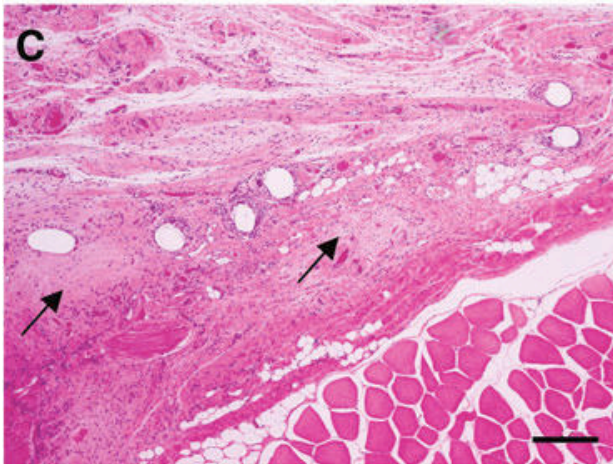
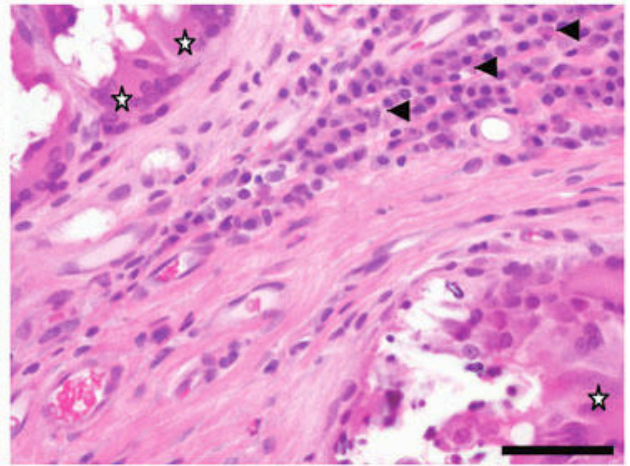
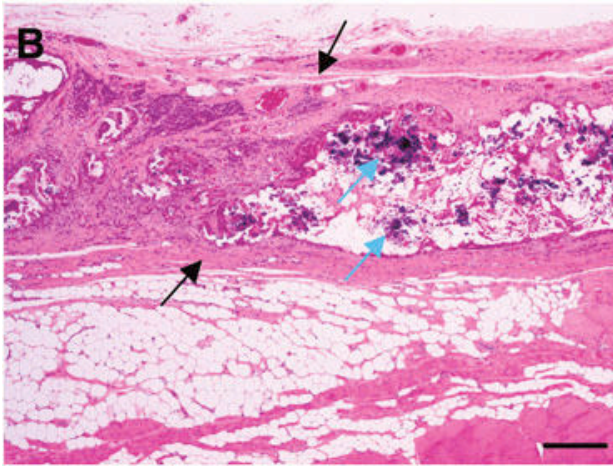
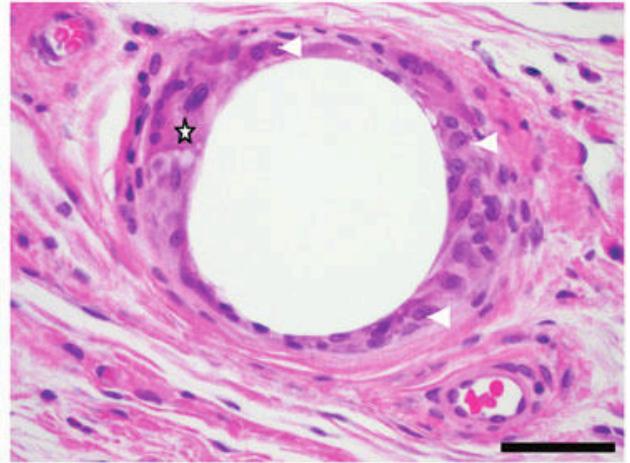
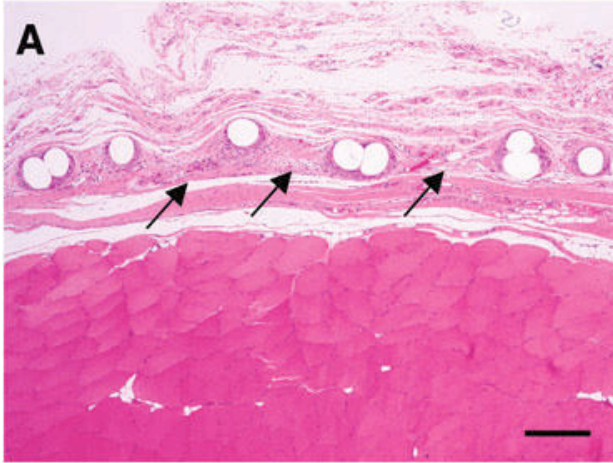


FIGURE 2.5. Comparison of representative tissue reactions to three test mesh articles at 12 weeks of post-implantation. (A) Ch-PPM. (B) PPM (Avaulta Solo, C.R. Bard, Inc.). (C) Col-PPM (Pelvitex; C.R. Bard, Inc.). Ch-PPM (A) is embedded in a narrow band of fibrous connective tissue (black arrows) and the individual fibers are cuffed by a moderate number of macrophages (white arrow heads) and multinucleate giant cells (star). In contrast, the PPM has invoked a severe inflammatory reaction and a wide band of fibrosis (between black arrows) with large foci of dystrophic mineralization (blue arrows). Note the large clusters of plasma cells (black arrow heads) and the numerous multinucleate giant cells (stars). The Col-PPM (C) is embedded in a wider band of fibrosis compared to the Ch- PPM (black arrows), but only a few inflammatory cells are present. All images in the left hand column taken at 4x magnification; scale bar = 500 mm. All images in the right hand column taken at 40x magnification; scale bar = 50 mm.

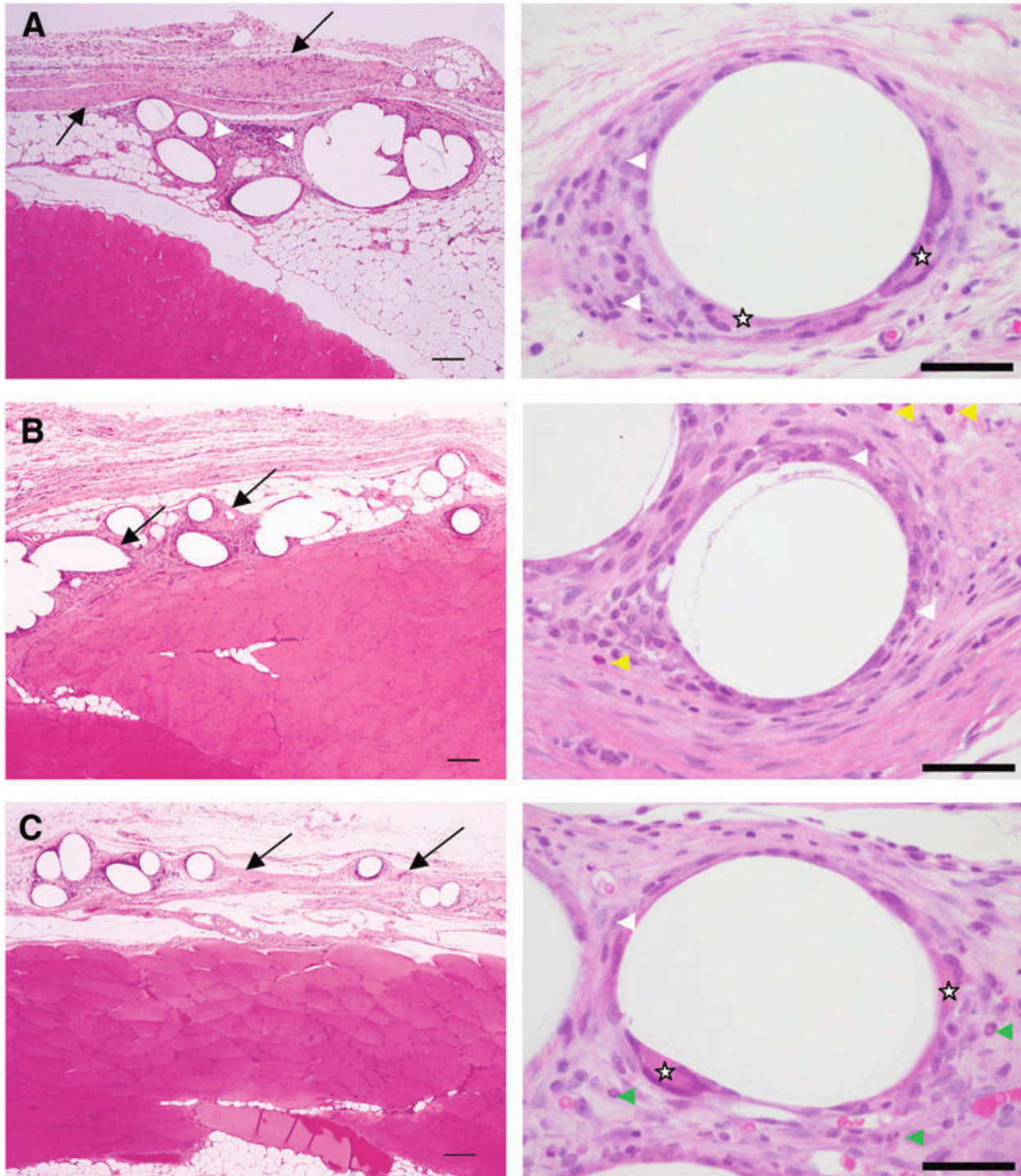


FIGURE 2.6. Tissue reaction over time to Ch-PPM. At 2 weeks (A) a thin layer of fibrosis (black arrows) and mixed inflammatory cells (white arrow heads), including neutrophils (green arrow heads), eosinophils (yellow arrow heads), macrophages (white arrow heads), and multinucleate giant cells (stars) surround the mesh. The degree of fibrosis is similar at 4 weeks (B) and 12 weeks (C), but the number of inflammatory cells is decreased and consists almost entirely of macrophages with rare multinucleate giant cells.

2.3.5 Macrophage Phenotype and Expression of Myogenin

Immunolabeling of representative sections from each sample group at 14 days post-implantation revealed qualitative differences in the phenotype of the cells at the interface with the mesh material (Fig. 2.7). All samples were associated with a similarly intense infiltration of CD68+ macrophages at 14 days. Both the PPM and Col-PPM groups were characterized by a predominance of CD86+ (M1 marker) cells both at the surface of the mesh and between mesh fibers. The Ch-PPM group was characterized by qualitatively fewer CD86+ cells at the mesh surface and peripheral to mesh fibers. PPM and Col-PPM samples were characterized by few CD206+ (M2 marker) cells at the mesh surface or between mesh fibers. The Ch-PPM group was characterized by the presence of CD206+ cells both at the mesh surface and peripheral to mesh fibers.

In Figure 2.8, immunolabeling of representative sections from each sample mesh type at 14 days post-implantation revealed qualitative differences in myogenin expression at the interface with the mesh material. Of the three mesh types, only the tissue samples with Ch-PPM were characterized with myogenin expression between mesh fibers. Expression of myogenin is limited to cells of skeletal muscle origin.

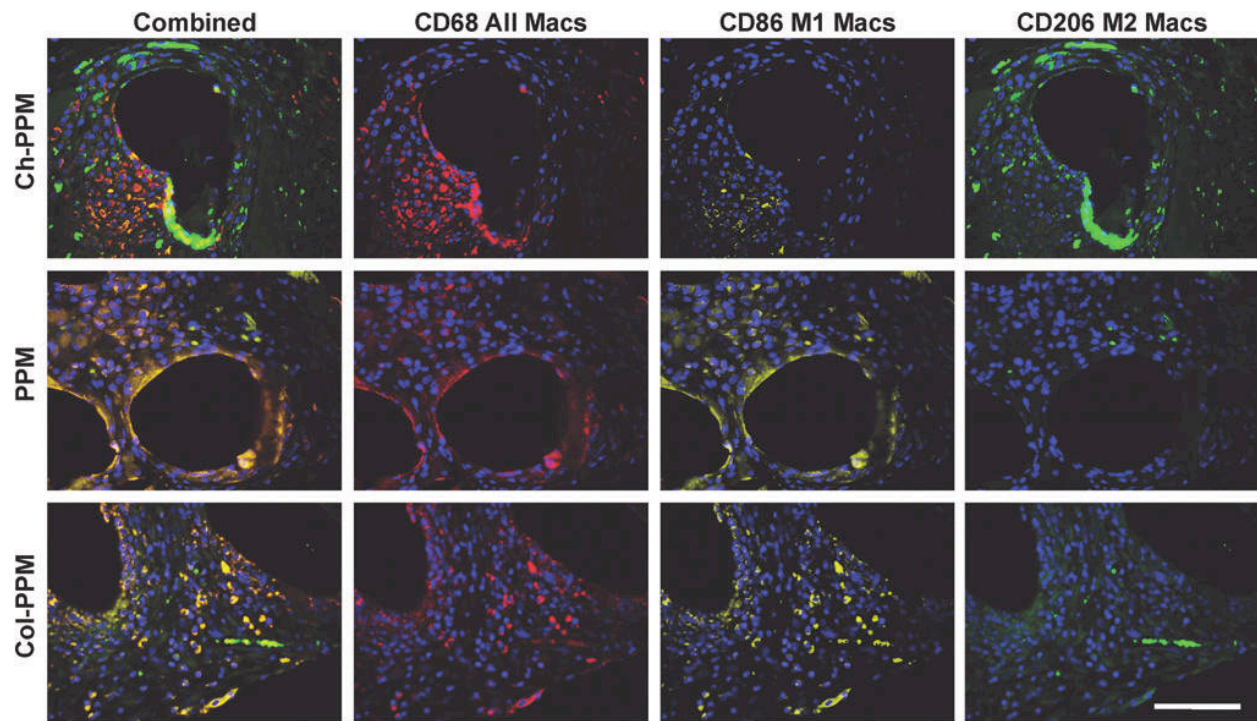


FIGURE 2.7. Immunolabeling of macrophage surface markers. Mesh materials were labeled with a pan macrophage marker (CD68, red), an M1 marker (CD86, yellow), and an M2 marker (CD206, green). All images taken at 40x magnification. Scale bar = 100 μ m.

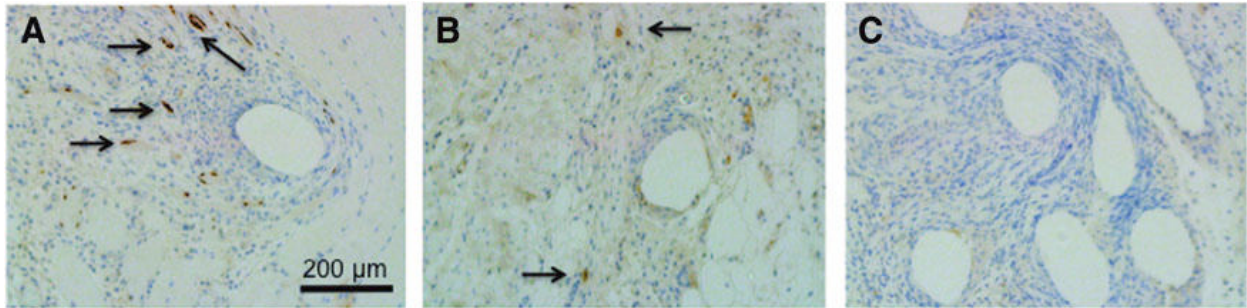


FIGURE 2.8. Immunolabeling of monoclonal mouse anti-myogenin of (A) Ch-PPM, (B) PPM, and (C) Col-PPM. Expression of myogenin (dark brown regions) is limited to cells of skeletal muscle origin and indicates early stages of muscle growth. Qualitatively higher amounts of positive stain of myogenin are seen in Ch-PPM (arrows). All images taken at 10x magnification.

2.4 Discussion

Implantable mesh materials for abdominal wall repair and pelvic organ repair should provide mechanical support and allow ingrowth of the surrounding tissues. In hernia and gynecological surgery, integration of muscle tissue into the mesh is desired to accommodate the natural contractility of the muscle on the abdominal wall or the smooth muscle in the vagina. It has been shown that the strength of polypropylene mesh is advantageous in abdominal wall implantation (88). However, after implantation of the mesh, substantial fibrosis and little or no functional muscle ingrowth is commonly observed around abdominal wall and/or the vaginal wall, despite providing adequate mechanical strength at the time of implantation. This causes significant differences in material properties at the mesh-native tissue interface, which could result in stress concentrations and stress shielding effects, leading to mesh erosion.

The objective of our study was to examine chitosan-coatings on polypropylene mesh to evaluate muscle tissue ingrowth and the inflammatory response. We

hypothesized that chitosan coating will promote muscle tissue ingrowth and decrease the inflammatory response. To test our hypothesis, an *in vitro* study was performed to determine the response of myoblasts and fibroblasts to different concentrations of chitosan coated on PPM. The *in vitro* results showed that the Ch-coating on PPM promotes myoblast and inhibits fibroblast attachment to the mesh. The *in vivo* study was then performed to further demonstrate that chitosan coating decreases inflammatory responses, promotes muscle tissue ingrowth and reduces fibrosis.

Polypropylene and various concentrations of chitosan were studied *in vitro* after myoblasts and fibroblasts were seeded 1:1, which mimics the *in vivo* environment where muscle and collagen fibers co-exist. A limitation of previous *in vitro* strategies for evaluating synthetic materials for muscle repair is their focus on a single cell type when evaluating the mesh materials. Many studies concerned with muscle cell attachment on mesh scaffolds seeded solely fibroblasts or solely myoblasts on the mesh (68,89,90). We believe, a co-culture of primary cultures of myoblasts and fibroblasts provides better evidence of how a mesh will perform *in vivo*. Preferential promotion of the attachment of myoblasts as opposed to fibroblasts in the co-culture environment may provide a better predictive metric to evaluate synthetic mesh materials *in vitro*.

The *in vitro* results that show the chitosan coating on polypropylene promotes myoblast early attachment over fibroblast attachment is further supported by *in vivo* observation that Ch-PPM generates significantly higher tetanic force, indicating the ingrowth of muscle fibers. The exact underlying mechanism of the effect is not clear. Diegelmann et al. postulate that one possible explanation may be related to microenvironment in response to chitosan (91). In their study, fibroblasts that appeared in the chitosan-treated polyvinyl alcohol (PVA) sponges were smaller and more circular

compared to the spindle-shaped fibroblasts observed in the control wounds. It is possible that chitosan may slow the attachment of fibroblasts. The SEM analysis suggests that the microarchitecture of the chitosan polypropylene offers greater surface area for cell attachment and smaller pores for cell entrapment when compared to the reference mesh, which is supported by our observation that cells were observed atop the chitosan coating in our *in vitro* portion of the study. The polypropylene serves as the skeleton and reinforced structure for the cells, and the microporous architecture of the chitosan sponge allows for easy cell attachment atop the interstices of the polypropylene knitted mesh. We believe that the higher force generation seen in the neo-tissue associated with the Ch-PPM group is due to functional muscle tissue ingrowth. As opposed to fibrotic tissue, functional muscle tissue will respond to electric stimulation to generate force. Both of force generation and assessment of myogenin expression confirm the ingrowth of muscle tissue in Ch-PPM. Other tissue integration will not cause such an enhancement. Additional studies are needed to understand how the number and arrangement of muscle fibers relate to *in situ* force generation observations.

Chitosan scaffolds induce only a minimal inflammatory reaction in a rat model. Although the material recruits neutrophils to the site of implantation, the neutrophils are not activated and the material induces neither lymphocyte proliferation nor antibody responses (48). Histopathological assessment of Ch-PPM implants in the present study found a moderate accumulation of primarily macrophages and fewer multinucleated giant cells at the implant-tissue interface that was unchanged from 2 weeks to 12 weeks post implantation. In contrast, the tissue reaction to PPM at 12 weeks consisted of a mixed mononuclear cell response that included varying numbers

of lymphocytes and plasma cells in addition to macrophages and multinucleated giant cells. Interestingly, at 12 weeks post implantation, a large sample of both the PPM and Col-PPM was surrounded by locally extensive areas of dystrophic mineralization, which was not observed around the Ch-PPM. Dystrophic mineralization typically occurs in necrotic or degenerated tissues. Our results suggest that chitosan coating alters the host immune response to the mesh resulting in decreased necrosis and tissue degradation. Further studies to confirm these observations and to elucidate the cellular and molecular mechanisms behind this change are needed.

To investigate the histology further, we conducted analysis of the macrophage phenotype at the mesh interface at 14 days post-implantation. A number of recent studies have demonstrated, despite the presence of large numbers of immune cells within the site of implantation at early time points (7-14 days post-implantation), some surgical materials are capable of promoting the formation of functional tissue while others elicit a foreign body reaction and tissue encapsulation. It has been suggested that these divergent outcomes are related to phenotypic differences in the macrophage population. The presence of a predominant population of M1 cells has been associated with poor remodeling outcomes, while M2 phenotype macrophages are associated with more integration and functional outcomes. Our results suggest that although a histologically similar population of predominantly mononuclear cells was observed at 14 days, Ch-PPM samples elicit a decreased M1 and increased M2 phenotype as compared to PPM and Col-PPM samples. These results are consistent with recent studies showing improved outcomes associated with materials which elicit an increased M2 response (56,75,92,93). These results coupled with the assessment of myogenin expression and the outcomes of the force generation testing favor Ch-PPM over

commercially available meshes. The mechanisms by which chitosan may alter the host immune response remain unclear, but appear to be associated with differences in long-term histologic outcomes.

Chapter 3

Biomechanical properties of mesh materials following implantation in the rat abdominal wall model²

3.1 Introduction

The 2005 National Health and Nutrition Examination Survey reports that the number of women in the United States with at least one pelvic floor disorder (PFD) will increase from 28.1 million in 2010 to 43.8 million in 2050 (94). Currently, women risk a 7% chance of requiring surgery for pelvic organ prolapse by the age of 80 (18). Re-operation, however, is common, with repeat cases reaching nearly 30% mainly due to complications of grafts used in female pelvic floor reconstruction (18). The magnitude of women who will be affected by PFDs emphasizes the importance of developing effective treatment strategies.

Common treatment options for PFDs, such as pelvic organ prolapse and stress urinary incontinence, involve insertion of classic biomaterials such as polypropylene

² Udpa N., Iyer SR, McDonough SP, Gao Y. "Type I and III collagen and biomechanical properties of

(PPM) (25,34,46,58,59,64,79,95–100). High failure rates, reported up to 40%, are associated with commercially available mesh, which has been reported to elicit a strong foreign body reaction and incompatible mechanical strength leading to discomfort in women³ when performing daily activities such as exercise, coughing, laughing, etc. (9,29,101). The complications are significant enough that the FDA issued warnings in 2007 and 2011 regarding the use of polypropylene mesh to treat PFDs (19,33,102).

The main function of the mesh insertion for pelvic floor reconstruction is to provide mechanical support to the pelvic tissues and organs. However, meshes come with their own set of complications. One theory for mesh failure is that stiffer meshes may increase the likelihood of erosion, pain, and poor function (103). In recent years, the center of attention for stiffness studies has shifted to alterations of the extracellular matrix (ECM). As the major component of the ECM and because of its high mechanical stiffness, the content and the ratio of collagen types I and III have been assumed to correspond with the tensile strength and mechanical stability of both the connective tissues and the scar tissue induced (104–107). Early phases of wound healing are characterized by the abundance of type III collagen, which is mainly replaced by mature, fibrillar type I collagen during later stages(108). Biological tissues with a high proportion of collagen type I (e.g. tendon) are characterized by greater strength and stiffness, and tissues with high levels of collagen type III (e.g. skin) are characterized by low strength (109). To avoid a mismatch of neo-tissue with native tissue, many studies have focused on evaluating the ratio of collages type I to type III to gain a sense of the

mesh materials following implantation in the rat abdominal wall model" (*in preparation*)

composition of the new tissue. With this in mind, researchers have suggested avoiding scaffolds and biological materials that elicit a low ratio of collagen types I to III as to indicate low mechanical strength and as a means to indicate people at high risk (104,110–112). However, more work is required to elucidate the relationship between the ratio of collagen types I and III and mechanical strength in urogynecologic meshes for pelvic floor repair.

Previous studies have shown that chitosan, a cationic polysaccharide showing excellent cell adhesive properties, influence the ratio of collagen types I/III in keloid fibroblasts (71). Additionally, there has been an emergence of literature in evaluating chitosan-based biomaterials as candidates for use in hernia and pelvic floor repair (38,64,65,81). The polysaccharide chitosan has been shown to be an effective biomaterial in a broad spectrum of applications due to its unique biological properties including nontoxicity, affinity for protein adsorption, antibacterial, hemostatic, fungistatic, and anti-tumoral properties (72), additionally, when using N-carboxybutyl chitosan in wound management researchers have found that it becomes gel-like in contact with the wound fluids, providing a bio-layer which provides a protection of the newly-formed tissues (113). Additionally, in a previous study, our lab showed that chitosan coatings preferentially promote the attachment of myoblasts over fibroblasts, have been shown to elicit a less fibrotic host tissue response *in vivo* (114,115).

The present study was designed to establish the relationship between collagen deposition and the mechanical properties of neo-tissue in a rat abdominal wall model after implantation of three different mesh types: a reference polypropylene mesh (Avaulta Solo®, C.R. Bard Inc., Covington, GA, USA), chitosan on polypropylene mesh, and a monofilament polypropylene mesh coated with hydrophilic porcine collagen

(Pelvitex™, C.R. Bard Inc.). The objective of our study was to 1) evaluate mesh strength and collagen incorporation after 4 and 12 weeks of implantation in a rat abdominal wall model and 2) determine the relationship between collagen deposition and mechanical strength of a chitosan-coated polypropylene mesh. We hypothesized that a reduction of the ratio between collagen types I and III of the neo-tissue results in a mechanically weaker tissue.

3.2 Materials and Methods

3.2.1 Overview of Experimental Design

All procedures were performed in accordance with the National Institute of Health (NIH) guidelines for care and use of laboratory animals, and with approval of the Institutional Animal Care and Use Committee (IACUC) at Cornell University. Male Wistar rats (Charles River Laboratories International, Inc.), weighing 250–450 g, were randomly assigned to nine groups of six each. Each rat was subjected to a partial thickness excision of a 1.2 cm x 1.2 cm section of the ventrolateral abdominal wall musculature on either side of the linea alba. The defects were repaired with one of the three test articles: polypropylene mesh (PPM), chitosan-coated polypropylene mesh (Ch-PPM), and collagen coated PPM (Col-PPM). The animals were randomly divided into 3 groups after surgery for survival of 2, 4, and 12 weeks. The harvested tissues were evenly split for measurement of tensile strength by uniaxial tensile testing and collagen typing. Native tissue was also tested as a control.

3.2.2 Preparation of Chitosan-coated Meshes and Characterization

To create and characterize the chitosan coatings we used the same methodology as described in an earlier publication (114). Briefly, we used high molecular weight chitosan, >75% deacetylated, ~600,000 MW (Sigma Aldrich, Milwaukee, WI) which was added to distilled H₂O at a 0.5% concentration (w/v) to a 1% (v/v) acetic acid solution until a clear solution was obtained. The sterile PPM was cut into 1.2 x 1.2cm squares and placed into a sterile bottle containing the 0.2µm-filtered chitosan-solution and stir bar. The mesh was removed from the solution, placed in a centrifuge tube, and left in liquid nitrogen for several hours while being placed in the lyophilizer at -40°C for 24 hours. The mesh samples were sterilized under UV light for 20 minutes. Scanning electron microscope (Leica 440, Buffalo Grove, IL) and Fourier transformation infrared spectroscopy (Bruker Vertex 80v, Billerica, MA) using Opus 6.0 Software was used to confirm the successful coating. PPM was also subjected to the same coating procedure ensure that the procedure does not affect the structure of PPM material.

3.2.3 in vivo Surgical Procedure

This procedure was described in a previous study from our lab (114) Each rat was anaesthetized using 2.5% isoflurane and an oxygen flow rate of 1 L/min. The ventral abdomen was clipped from the xiphoid process to the pubis, and sterile prepped with povidone-iodine scrub and warm saline. A 4cm ventral midline abdominal skin incision was made, and the skin and subcutaneous tissue were separated from the underlying musculature. Bilaterally, a 1.2 cm x 1.2 cm section of the external and internal abdominal oblique layers of the ventrolateral abdominal wall was

excised while the underlying transverse abdominus and peritoneum remained intact. Different test articles were placed in the ventrolateral defects and oriented with the weave pattern perpendicular to the linea alba. The defect was repaired with a size-matched piece of the chosen test article that was randomly selected prior to surgery. PROLENE™ sutures (Ethicon Inc., Somerville, NJ) were placed at each of the four corners of the test article to secure the mesh to the surrounding musculature. A MONOCRYL™ suture (Ethicon Inc.) was used to close the skin incision. Each animal was recovered from anesthesia and returned to the housing unit. Each rat received meloxicam and general health status and surgical site were monitored daily post-implantation.

3.2.4 Collagen Typing

In the first group, after rats were euthanized, constructs were dissected off. The collected tissues with constructs were fixed by immersion in 10% neutral buffered formalin, embedded in glycol methacrylate (GMA), sectioned at 3 um and stained with picosirius red using standard histological techniques. Each section was examined by a board certified veterinary pathologist (SPM) who was blinded to the treatment groups. The sections were analyzed using an Olympus BX41 microscope (Melville, NY, USA) equipped with filters to provide circularly polarized illumination and aligned so that the background in the field of view was as dark as possible (i.e. crossed polarized light illumination). Digital images obtained with a 10X objective lens and a digital camera (DP21, Olympus) were captured as TIFF files at 1600 x 1200 pixels at a resolution of 60 pixels/cm and displayed on a high-resolution monitor (Dell 2408WFP).

To ratio the samples for the collagen type I/III ratios, a board-certified veterinary pathologist, blinded to the mesh samples evaluated the yellow pixels (collagen type I) and green pixels (collagen type III) using a proprietary color de-convolution algorithm (Aperio, Vista, CA, version 9.1) that separates the image into three channels that correspond to the colors of the stain used. The input parameters, optimized according to the manufacturer's instructions, for each color and the background (channel 1 = yellow, channel 2 = green and channel 3 = background) were as follows: channel 1) red component 0, green component 0.062, and blue component 0.451, channel 2) red component 0.243, green component 0.12 and blue component 0.231 and channel 3) red component 0.402, green component 0.541 and blue component 0.567. Four to eight regions within the interface were captured by the camera for each mesh sample and the collagen I/III ratios were obtained by analysis of the amount area of collagen type I and III. Results are expressed as a collagen types I/III.

Additionally, for each sample we calculated the volume fraction of collagen type I and type III using the same de-convolution algorithm to determine the amount of collagen within the total area selected. Four representative regions per sample were selected.

3.2.5 Uniaxial Tensile Testing

In the second group, after the rats were euthanized, a uniaxial tensile test in the longitudinal direction was performed. After sacrifice, the samples were carefully dissected from the surrounding connective tissue and immediately stored at -80°C. On the day of testing, the tissue was cut using a custom-made dogbone punch

(length/width aspect ratio = 3) and thawed immediately before performance of the uniaxial tensile test in a water bath. Native tissue was dissected off the samples and soft-tissue clamps lined with sandpaper were utilized to grip each sample at the proximal and distal ends. Throughout the experimental protocol, the sample was kept moist using 0.5% saline. The distal end was attached to a 1kg load cell (Honeywell model 31, resolution 0.1 N; Sensotec, Columbus, OH) and secured to the base of the uniaxial testing machine EnduraTEC loading frame [EnduraTEC; Electroforce (ELF) 3200 System, Minnetonka, MN]. The specimen was aligned with the loading axis of the machine. A small preload (0.1 N) was applied to the tissue and 10 cycles of preconditioning was performed at a rate of 10 mm/min. A load to failure test was performed immediately after the preconditioning, as previously described (76).

Several metrics were collected: the load (force, N) and elongation (distension, mm) of the tissue were recorded and used to generate load-elongation curves, which were then converted to a stress-strain relationship to calculate the mechanical properties of the vagina in the longitudinal direction. Stress was defined as the load (a measure of the force applied to the tissue) divided by cross-sectional area, and strain was defined as the change in distance between the clamps divided by the original distance between the clamps ($\Delta l/l_0$). The slope of the linear region of the stress-strain curve was defined as the tangent Young's modulus (a measurement of stiffness), while the ultimate tensile strength and maximum strain were recorded at failure (point at which the specimen breaks apart).

3.2.6 Statistical Analysis

All data was analyzed with JMP (v.9) using a mixed model. Statistical analysis was done using a mixed model with student t-test comparison ($n = 8, p < 0.05$). Fixed effects tests were done on mesh type, time, and mesh type cross time. Differences between mesh samples were analyzed using a student t-test with a Bonferroni correction for nine comparisons (4 weeks, 12 weeks, and comparisons between time points) in cases where there was significant difference ($p\text{-value} < 0.05$). All values are expressed as the least mean square mean \pm standard deviation.

3.3 Results

3.3.1 Analysis of Collagen Typing

The total volume fraction of absolute amounts of collagen types I & III deposited in the neo-tissue was similar [4 weeks: Ch-PPM (0.498 ± 0.13), PPM (0.508 ± 0.1), Col-PPM (0.419 ± 0.08); 12 weeks: Ch-PPM (0.513 ± 0.15), PPM (0.495 ± 0.19), Col-PPM (0.577 ± 0.34)]. There was no significant difference noted between mesh types or time points. This data is consistent with previous work shown in our lab shown in Table 2.2 in Chapter 2, specifically the width and amount of fibrosis for each implant. Table 3.1 summarizes the ratio of collagen type I/III of the mesh samples after implantation in the abdominal wall. Again, there was no significant difference between the mesh samples at both time points or between mesh samples; however, we witnessed a clear trend with incorporation of more collagen III, lower collagen type I/III ratio, from 4 weeks to 12 weeks across all mesh types.

Figure 3.1 illustrates the picrosirius red staining of mesh samples at 4 and 12 weeks post implantation.

TABLE 3.1 Ratio of collagen I/III ratios in mesh samples

Group	N =	4 weeks	12 weeks
Ch-PPM	8	0.938±0.719	0.600±0.356
PPM	8	0.663±0.531	0.327±0.239
Col-PPM	8	0.637±0.294	0.826±0.486

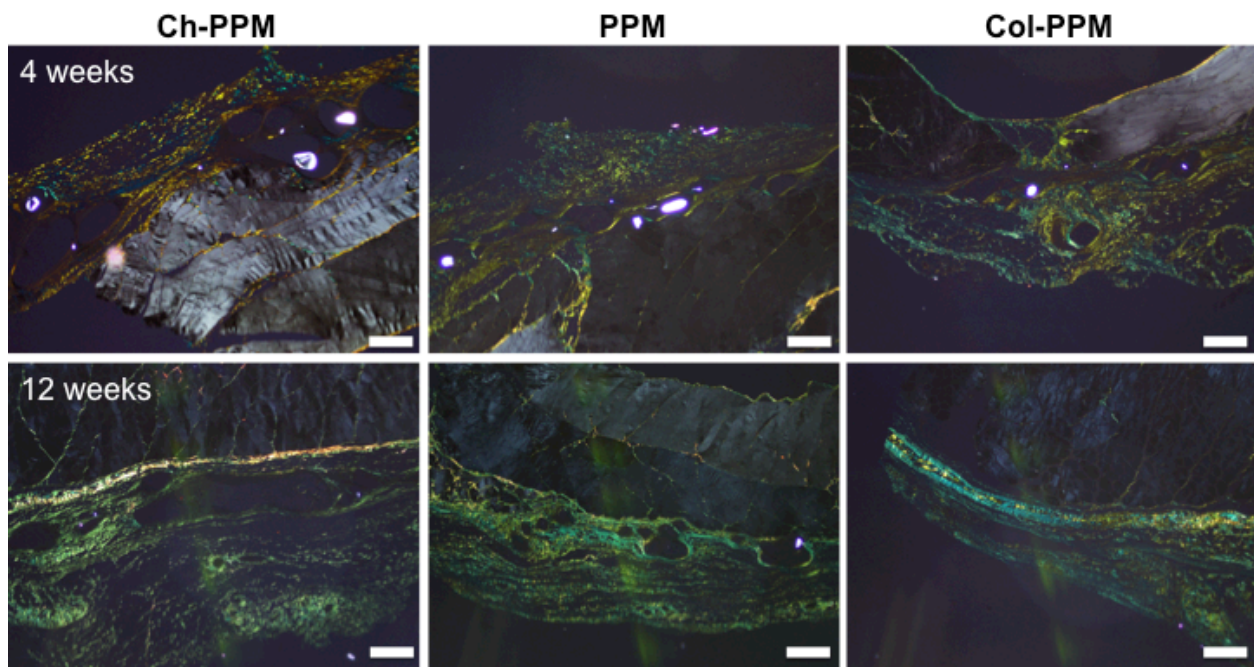


FIGURE 3.1. Mesh samples explanted after implantation. Visualization by crossed Polaroid filters allowed estimation of collagen type I, seen as thick yellow, orange or red colored fibers and collagen type III fibers are thinner and stained in pale green shades. Magnification 4x. Scale bar: 500 μ m. Gray portions indicate native tissue.

3.3.3 Analysis of Uniaxial Tensile Testing

The biomechanical properties of the urogynecologic mesh samples are reported in Table 3.2 and representative curves are shown in Figure 3.3. The curves exhibit a non-linear shape, which can be divided into 3 regions: 1) the initial non-linear toe region; 2) the linear region; and 3) failure region. For all meshes, during pre-conditioning, the first cycle indicated a pronounced toe region (i.e., low stress), which lessened in the consequent cycles. At 4 weeks, we noticed that the onset of the linear region varied between mesh types. Col-PPM had a much larger toe region with the linear region starting at 25-60% strain in comparison with PPM and Ch-PPM, starting at 15-25% strain and 10-25% strain, respectively. It suggests that the collagen fibers may be kinked or may be orienting in a direction that is perpendicular to the longitudinal direction. At 12 weeks, we notice that the PPM does not reach the linear region until 30-40% strain, while both Ch-PPM and Col-PPM have linear regions starting at 15-30% strain.

No infection or erosion of any of the mesh samples occurred in the abdomen. There was no effect of time between samples. After 4 weeks of implantation, Ch-PPM ($p = 0.001$) and PPM had a significantly higher ultimate tensile strength in comparison with Col-PPM. At 4 weeks, Ch-PPM ($p = 0.001$) also had a significantly higher elastic modulus than Col-PPM. Between 4 and 12 weeks, Col-PPM is the only mesh sample that became significantly stiffer ($p = 0.02$). At 12 weeks after implantation, Ch-PPM was had a significantly higher ultimate tensile strength in comparison with PPM ($p = 0.003$) and Col-PPM ($p = 0.02$). Considerable variation in tensile properties with a mesh type may be related to the degree of degradation and host tissue incorporation.

TABLE 3.2. Comparison of tensile properties of neo-tissue after implantation of mesh at 4 and 12 weeks

	Elongation at failure (%)	Ultimate tensile strength (kPa)	Elastic Modulus (kPa)	Thickness (mm)
4 weeks				
Ch-PPM	55±7.0	1596.34±147.24 ^Y	4674.83±2663.6 ^Y	0.45±0.15
PPM	81±12.4	2125.29±588.03 ^Y	3388.20±567.36	0.49±0.15
Col-PPM	88±29.2	813.02±235.97	2203.15±1107.7 ^{8*}	0.36±0.11
12 weeks				
Ch-PPM	68±17.9	4543.64±1254.18 ^{β, Y}	8264.1±1753.63	0.45±0.22
PPM	75±8.9	2317.13±267.53	4469.53±909.86	0.42±0.07
Col-PPM	76±20.7	2199.55±809.08	5005.68±614.57	0.43±0.17

'β' indicates significantly different from PPM within time point; 'γ' indicates significantly different from Col-PPM within time point; "*" indicates significantly different from same mesh type at 12 weeks

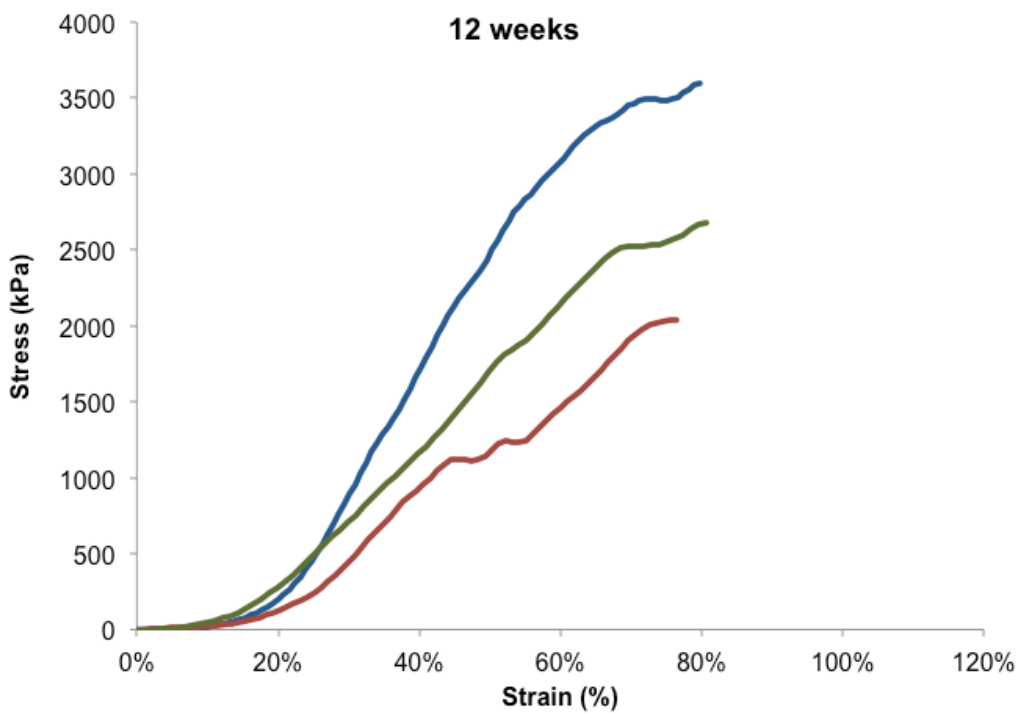
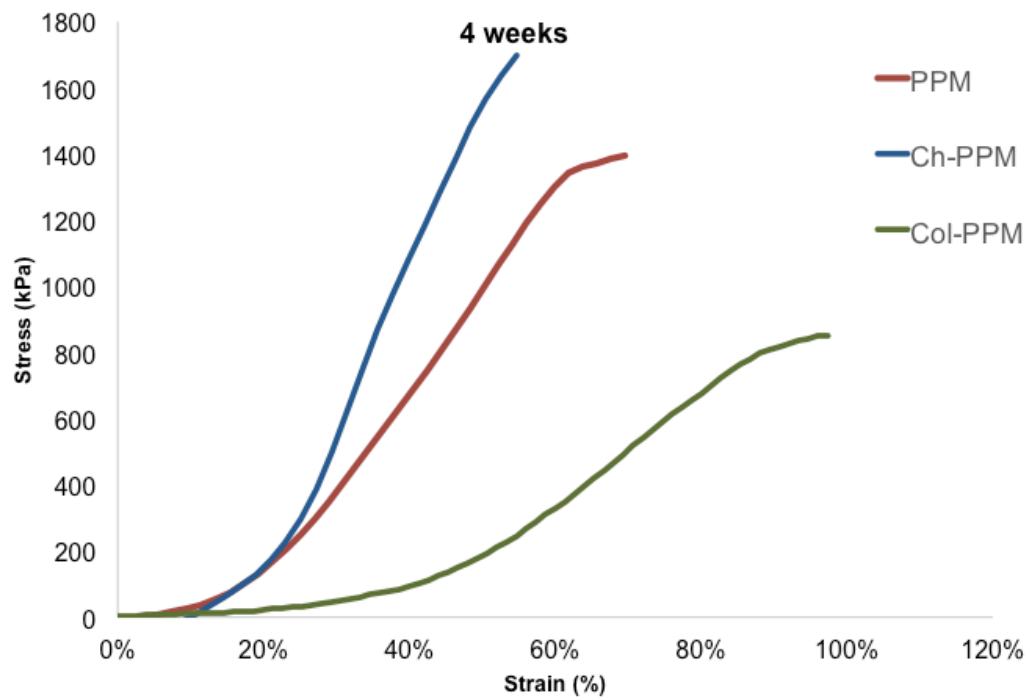


FIGURE 3.3. Representative stress-strain curve of mesh samples. (A) Ch-PPM, PPM, & Col-PPM at 4 weeks; and at (B) 12 weeks.

3.4 Discussion

Mesh materials for repair of pelvic floor and hernia repair have become integral components in surgery and are nowadays regarded as standard procedures for treatment. Ideally, surgical mesh materials for hernia and pelvic organ repair should provide mechanical support, accommodate the natural contractility of muscle, and allow for adequate collagen deposition during wound healing (34).

Within the first phases of wound repair processes, tissue formation is characterized by fibroplasia, neovascularization and ECM production. Later phases of wound repair are characterized by matrix remodeling with remodeling of initial granulation tissue into connective tissue. The initially abundant immature type III collagen is for the most part replaced by mature type I collagen during the physiological wound healing. The relative proportions of types I and III and distribution have been studied in a number of studies (112,116–120). It has been suggested that the presence of type III collagen and its relative proportion correlates with strength of the newly formed tissue, though to our knowledge, there have been no studies that have demonstrated the correlation between the mechanical strength experimentally in a single study(121). The objective of our study was to 1) evaluate mesh strength and collagen incorporation after 4 and 12 weeks of implantation in a rat abdominal wall model and 2) determine the relationship between collagen deposition and mechanical strength of a chitosan-coated polypropylene mesh. We hypothesized that a reduction in the ratio between collagen types I and III of the neo-tissue would result in a mechanically weaker tissue.

Our results suggest that coating the meshes with biological materials does not significantly impact the collagen type I/III ratio. The determined ratio in our samples

illustrates that the primary collagen found in the implanted meshes is collagen type III in comparison with collagen type I. Structures, like the pelvic floor, that necessitate distensibility, consist of predominantly collagen type III(47,118). Lehto *et al.* found that native rat abdominal wall muscle has a collagen type I/III ratio of 0.37, which is fairly close to the neo-tissue score surrounding PPM(122). These results are consistent with our previous study that showed using a semi-quantitative histopathological assessment to examine the fibrotic response of the three mesh types that there was no significant difference (114). Junge *et al.* have also shown no significant differences in the collagen type I/III ratio between mesh samples varying in pore diameter, weight, structure, and material in a rat abdominal wall model (123).

We found that the Ch-PPM mesh is significantly stiffer than the commercially available meshes at both 4 and 12 weeks. The results of our uniaxial tensile testing for PPM and Col-PPM are consistent with literature(76). While there was no significant difference in elongation or thickness of newly formed tissue, we observed that Ch-PPM had a higher ultimate tensile strength at 12 weeks in comparison with PPM and Col-PPM. This does not correlate with our data for the collagen type I/III ratio; therefore, we conclude that there is no relationship between the collagen type I/III ratio. As no significant differences are observed on absolute collagen content, the higher stiffness of Ch-PPM is not due to the absolute content of collagen in the mesh. Ideally, the strength and elasticity of surgical mesh materials used for pelvic floor repair should match the native tissue in order to support to pelvic organs and minimize erosion (76). In addition to collagen concentration, biomechanical properties also depend on cross-link density. Thus, high stiffness of neo-tissue with implanted Ch-PPM could be due to a higher cross-linking density (54,124).

The other possible reason for higher stiffness of Ch-PPM mesh could be the orientation and geometry of the collagen fibers in the tissue. In many soft tissues, a nonlinear stress strain relationship is observed for all three types of mesh. The stress strain curve is characterized by a toe region, in which the stiffness increases with increased strain, a linear region, and a failure region. The toe region suggests that the collagen fibers may be crimped or might be oriented in a direction that is perpendicular to the longitudinal direction(125). When the tissue is stretched, the collagen fibers straighten and reorient to the direction where the load is applied. When most the fibers are straight, and reoriented, the stress strain relationship becomes linear. Therefore, the size of the toe region indicates the waviness and orientation of collagen fibers in the tissue. Our *ex vivo* uniaxial tensile tests showed that at 12 weeks, the PPM has a larger toe region with the linear region starting at 30-40% strain, while both Ch-PPM and Col-PPM have linear regions starting at 15-30% strain, suggesting that the collagen fibers in Ch-PPM are either more straight or orient more along the direction that load applies. This is supported by previous studies that suggested chitosan is able to enhance vascularization and a continuous supply of chitoo-ligomers to the wound that stimulate correct deposition, assembly and orientation of collagen fibrils, and are incorporated into the ECM (71). Therefore, the high stiffness of Ch-PPM mesh could be due to the different range of the toe region suggested that the waviness and orientation of the collagen fibers.

Coupled with our previous study, we believe that the additional mechanical strength found in samples implanted with Ch-PPM, could also be due to an increase in muscle fibers, which in addition to generate active muscle force, also contribute to passive mechanical strength. In our previous study, we have shown that chitosan

coating on tissue culture plates or polypropylene promotes attachment of myoblast *in vitro* (114,115). We also showed that chitosan coating on polypropylene mesh promotes muscle tissue ingrowth *in vivo*, demonstrated by higher amounts of immunolabeled myogenin and higher muscle force generation in Ch-PPM samples after implantation in a rat model(114,115). Therefore, we believe that the muscle tissue ingrowth into the neo-tissue surrounding the Ch-PPM mesh is also responsible for the higher elastic modulus. This is indirectly supported by a previous finding that when muscles are compromised by disease or age, damaged muscle fibers are instead replaced by infiltrating fibrous tissue or fat, leading to a net loss of muscle mass and as a result, a loss of strength(68).

Limitations of this study exist. The circular polarized light technique we use to evaluate collagen deposition has its limitations. For one, it is only an estimation of the ratio of collagen types, in contrast to a biochemical analysis. Though this method is widely used and accepted, if polarized light is used, it is possible that some collagen fibers will not appear if they are aligned parallel to the transmission axis of either of the two polarizing filters. A rotating microscope stage can minimize this effect; however, collagen fibers are frequently crimped or wavy. Thus, some fibers will appear dark no matter how the microscope stage is rotated. Thus, total collagen content may be underestimated, especially in tissue containing large amounts of wavy fibers (126). However, we have minimized this effect by taking the ratio of the collagen types and we assume that both collagen I and collagen III fiber may not be visible to alignment with the transmission axis equally. Data from this study was obtained from a rat model using a relatively small sample size. In a review published by Goh (2003), the author discusses the limitations of the uniaxial tensile testing of mesh samples for prolapse repair, stating that the ultimate tensile strength is not the strongest indicator of whether

a mesh will fail since under normal physiological conditions the tissue may not undergo failure due to elongation. However, in order for clinicians to select the appropriate mesh for a patient, it is critical to first characterize the meshes' biomechanical properties and biochemical content.

In summary, we have characterized the collagen deposition and tensile properties of two different meshes used for pelvic floor repair as well as a chitosan-coated polypropylene mesh for comparison. We found that neo-tissue after implantation of Ch-PPM is stiffer than commercially available mesh used in a rat abdominal wall model. We also observed no significant difference in the ratio of collagen types I/III between mesh samples at 4 weeks or 12 weeks, and we did not find a relationship between the collagen type ratio and the mechanical strength of mesh samples after implantation. We believe that high stiffness observed with the Ch-PPM could be due to the waviness or orientation collagen fibers and higher content of muscle tissue. We plan on building on this work and studying the orientation of the collagen fibers after implantation as well as quantifying the density of the cross-linking and collagen fiber concentrations biochemically.

Chapter 4

Conclusion and Future Work

4.1. Conclusion

Over the last decade, surgical mesh has been widely used to reconstruct the pelvic floor, treating conditions like cystoceles (bladder prolapse) and uterine prolapse. Surgical mesh was introduced on the basis that it may provide a more durable repair than traditional procedures. Epidemiology studies have shown that while serious complications are uncommon, they are difficult to treat, have a high re-operation rate, and occasionally cause permanent disability, even after removal of the mesh. Long-term cure rates after implantation of mesh for pelvic floor disorders continue to be suboptimal and may be due to a mismatch of neo-tissue and native tissue strength, inadequate tissue ingrowth, or rejection of a foreign body. In order to develop a new generation of mesh and get a more complete picture of surgical mesh intended for pelvic floor repair, the mechanical properties, inflammatory response, and especially functional muscle growth must be evaluated. Ideally, this data allows surgeons to tailor their mesh selection based on patient needs.

In addition to providing support to organs, meshes intended for pelvic floor reconstruction or abdominal hernia repair must achieve a high level of tissue incorporation while averting unwanted side-effects (127). One of the complications of using synthetic materials for muscle tissue reinforcement is excessive fibroplasia. Fibrous capsule formation inhibits the integration of the implanted material within the

tissue of interest and leads to a mismatch in mechanical properties with natural tissue, leading to a reduction of function and discomfort (75,128), which may require corrective surgeries due to complications including mesh erosion and mesh exposure among others. Ideally, mesh intended for pelvic floor repair, when implanted, will allow for muscle tissue ingrowth and will match the mechanical integrity of native tissues without significant granulation tissue and or fibrosis. Materials, which preferentially promote the attachment of myoblasts over fibroblasts, may elicit a less fibrotic host tissue response *in vivo*.

In this thesis, the effects of chitosan coating on polypropylene mesh were evaluated for preferential attachment of muscle tissue as well as response after implantation in a rat abdominal wall model in comparison with commercially available mesh.

The results of this thesis indicate that chitosan coatings may be highly suitable for use in pelvic floor repair and there are a considerable number of indicators to measure success in an animal model. This thesis worked towards bridging the fields of engineering and urogynecology by characterizing two commercially available meshes and introducing a chitosan-coated mesh for comparison. While the PPM and Col-PPM samples are commercially available surgical options, the differences in the contractile response and tissue integration are very different from one another. In comparison, we found that the Ch-PPM has a higher elastic modulus than both commercially available meshes. Compared to the Ch-PPM, we also see remarkable differences in macrophage phenotype, myogenin expression and tetanic force generation. We concluded that chitosan is a promising candidate coating for urogynecological materials due to its

ability to promote muscle tissue ingrowth and decrease the inflammatory response. More work is required to show how chitosan coated mesh performs in a large animal vaginal wall model (see Future Work). However, with marked differences between the properties of the three meshes in this thesis, this research should encourage engineers and clinicians to re-examine what properties likely lead to complications like mesh erosion, exposure, pain, etc., so that the appropriate mesh can be selected for patient use.

The first half of Chapter 2 is centered around an *in vitro* study which showed that polypropylene meshes coated with 0.5% or 0.7% chitosan preferentially enhance the attachment of myoblasts when seeded 1:1 in co-culture with fibroblasts. The microporous structures made of chitosan in the interstices of the polypropylene mesh also allowed for better cell attachment. The polypropylene, served as the skeleton, while the lyophilized chitosan gel provided the cells with a microporous structure. Both 0.5% and 0.7% Ch-PPM developed in this study may lead to an improved biomaterial for muscle repair applications. By utilizing chitosan as a coating that increases the myoblast to fibroblast attachment, this study showed that the implanted mesh will reduce fibroplasia *in vivo*. While many studies have evaluated the effects of chitosan-based biomaterials for dermal healing and cartilage and bone growth, this study was one of a handful to evaluate the effects of chitosan on myoblast and fibroblast cell attachment.

The second half of Chapter 2 is focused on selecting the mesh that preferentially attached myoblasts over fibroblasts *in vivo*, and evaluating for functional muscle tissue when introduced to a rat abdominal wall model. We hypothesized that Ch-PPM will promote muscle tissue ingrowth and decrease inflammatory response in a rat

abdominal wall model. The first metric we checked for was muscle ingrowth, which we tested two ways: functional muscle testing and myogenin expression. The second metric we examined was for severity of inflammatory response, which we tested two ways: through H&E staining and Immunolabeling of macrophage surface markers. We found that Ch-PPM promotes tissue ingrowth. Functional muscle testing showed that 0.5% Ch-PPM generates significantly higher tetanic force than PPM. Additionally, neo-tissue surrounding Ch-PPM was characterized by myogenin expression between mesh fibers. Ch-PPM induced moderate inflammatory response. Histology showed a narrow band of fibrosis with a high number of macrophages. We immunolabeled the mesh samples for macrophages and found the presence of CD206+ M2--the presence of which is believed to lead to better remodeling outcomes with anti-inflammatory, regulatory and wound healing properties. This research showed that chitosan could be a viable option for skeletal muscle repair. Chapter 2 is the first study of its kind to use an early *in vitro* metric to evaluate muscle growth and see how if it led to functional muscle growth *in vivo*. Evaluating neo-tissue for muscle tissue ingrowth may decrease the mismatch in properties between native tissue and neo-tissue post-mesh implantation. Future research in this field may consider evaluating the myoblast to fibroblast ratio as an early indicator before beginning *in vivo* studies. Additionally, the ratio of myoblasts to fibroblasts *in vitro* may be a predictor for success in an *in vivo* environment.

Chapter 3 continues on our work from Chapter 2 with the same abdominal wall model in a rat. We had a two-part aim for this study: (1) obtain information about the mechanical properties of Ch-PPM, and (2) establish the relationship between the ratio of collagen types I/III and mechanical properties after mesh samples are implanted in a rat abdominal wall model. We hypothesized that Ch-PPM neo-tissue will approach the

strength of native tissue better than commercially available mesh, and that the ratio of collagen types I/III can be used to predict the mechanical properties of neo-tissue in a rat abdominal wall model. To do this we did both *ex vivo* uniaxial tensile testing and collagen types I/III staining using picosirius red. Results showed that using the ratio of collagen types I/III areas should not be used as a predictor for mechanical strength for all mesh types at both time points, however the score may be a better indicator. We also found that the ultimate tensile strength and elastic modulus were significantly higher for Ch-PPM at 12 weeks. This was the first study of its kind to characterize the mechanical properties and collagen deposition of a chitosan-coated mesh. It was also the first to evaluate the relationship between the collagen type I/III ratio and mechanical properties of neo-tissue after mesh implantation in an abdominal wall model. In this study, we contend that prior to determining the success of a mesh in clinical studies, one must have a comprehensive understanding of its mechanical behavior. A mismatch in properties between neo-tissue and native tissue may be a likely reason for failure of mesh or recurrent prolapse. By improving our understanding of the differences between meshes after host incorporation, we will have a foundation upon which to base differences in the behavior of meshes that may occur in clinical applications.

Improved urogynecological meshes have the potential to improve our long-term success rates (100,129). The challenge in prolapse surgery is that while the prolapse itself may cause difficulties with bladder, bowel and sexual function, surgical correction may also affect these functions in unpredictable ways. By improving our understanding of the differences between meshes after implantation in a small animal model, we will have an enhanced understanding upon which to select the appropriate mesh for clinical

use. Recent progress in skeletal muscle wound management is mainly in terms of physiologic support of healing (71). Chitosan substantially contributed to research advances in the field of biomaterials. Improving the appearance and functionality of regenerated tissue in wounds may benefit from the versatility, functionality and efficacy of chitosan.

4.2. Future Work

This thesis raises many more questions than it answers. There are several exciting lines of research arising from this work that should be pursued and our lab is interested in pursuing research in three areas: 1) a mechanism study to understand the relationship between chitosan substrate and cell attachment; 2) an analogous large animal study to understand the effects of chitosan on smooth muscle of the vaginal wall; and 3) measure the anisotropic properties of the tissue using biaxial testing in a large animal model.

First, there is no perfect animal model substitute for humans. Thus, the selection of an animal model is mainly driven by the research topic under investigation. However, with very little data available on the biomechanical behavior of animal models related to vaginal and pelvic floor function, the choice of a specific animal model can be difficult. Typically, after a small animal model, researchers progress to a larger animal model. In our case, it is necessary to continue our work in a larger animal model with functional anatomy similar to humans. Interestingly, the sheep has been evolving as a model for evaluating prolapse (3), and similar to women, uterovaginal prolapse occurs commonly in sheep. Sheep are an established reproductive model for humans, with long labors with large fetuses. Additionally, sheep spontaneously develop pelvic organ prolapse related to pregnancy and vaginal birth (130–132).

Abramowitch *et al.* conducted a review of animal models for PFD repair and his group discovered that pelvic anatomy and morphology in sheep are remarkably similar to humans and may be an appropriate alternative to the expensive and less accessible primate model (Fig. 4.1) (3). Additionally, added vascularity and presence of microflora in the vagina may have further impact on the host tissue response and biomechanical properties of materials used in vaginal repair relative to materials used for abdominal repair (133). A sheep model would also allow for a long-term study to be conducted and for vaginal placement as opposed to abdominal placement. This proposed study would be the first of its kind to study chitosan coated meshes in an ovine model and would be a more thorough assessment of collagen and elastin content deposition after implantation in the vaginal wall.

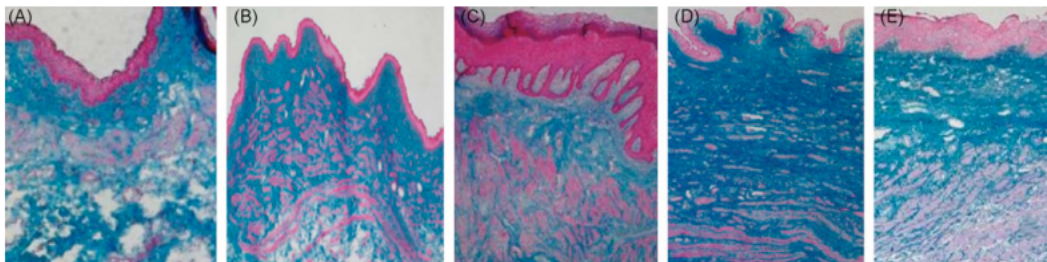


FIGURE 4.1. Histological trichrome images indicating the difference in morphology of the animal model from L to R (A) rat, (B) rabbit, (C) primate, (D) sheep, with respect to humans (E). The thickness of the epithelium varies among the animal models and with respect to human. However, it is evident that the vaginal wall of the sheep (D) holds a high degree of similarity to the human vaginal wall (E).(3)

To move toward characterizing the anisotropic behavior of planar tissues such as the vagina, biaxial testing must be performed on ovine tissue samples in which stress or strain can be applied simultaneously and independently along two orthogonal axes (Fig. 4.2). A limitation in Chapter 3 is the method of uniaxial testing. Though it

permitted us to characterize and compare the mechanical properties of the coronal plane of the rat abdominal wall, to advance the state of the field, biaxial testing in the longitudinal and circumferential axes must be completed on ovine vaginal tissue after implantation of mesh samples. Planar biaxial testing of vaginal tissue may provide a more complete characterization of the remodeling and effects of pregnancy, vaginal delivery, and birth injury (134). Constitutive models, described by Sacks *et al.*, should be implemented into a finite element analysis to assess the behavior of the vagina under a variety of parameters (135,136).

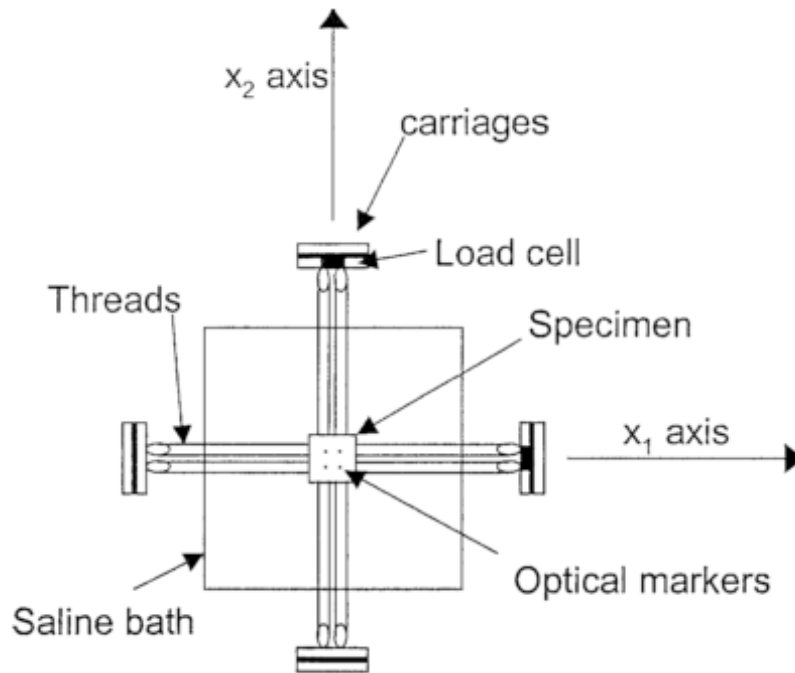


FIGURE 4.2. Schematic of a biaxial testing device (131)

Finally, further studies to elucidate the cellular and molecular mechanisms behind chitosan coatings and cell attachment. Cell surface receptors, such as integrins are crucial for adhesion of cells to a substrate as they recognize adsorbed ECM proteins leading to adhesion and reorganization of actin and cellular cytoskeleton. Future studies should be performed to elucidate the molecular role of substrate and cell adhesion molecules. Substrates have previously been observed to play an important role in protein adsorption and cell adhesion. *In vitro* work in our lab has shown that an organized actin and integrin β_3 network around the nuclei of myoblasts was observed with chitosan, whereas disrupted actin and integrin β_1 network was observed under the same conditions for fibroblasts. Our lab concluded that chitosan promotes myoblast

adhesion by higher expression of integrin β_3 and inhibits fibroblast adhesion due to disruption of actin and integrin β_1 network. However, the interaction between chitosan, and adsorption of ECM proteins and integrin β_3 and integrin β_1 can be further analyzed to determine the molecular mechanisms behind the selective adhesion of myoblasts over fibroblasts. The effect of chitosan on polarization of macrophages and collagen deposition can also be analyzed to optimize skeletal muscle regeneration.

APPENDIX I: in vitro protocols

How to Harvest Fibroblast Cells from CD-1 Mice

1. Sacrifice 1 adult CD-1 mouse by CO₂ inhalation.
2. Spray 70% ethanol on skin to disinfect.
3. Use #10 disposable scalpel and sterile scissors to remove hair and reveal skin.
4. Skin biopsies are taken using a 3mm to 5mm diameter sterile biopsy punch.
5. Using another sterile #10 disposable scalpel finely chop the biopsy into 1mm pieces.
6. Put 2 mL Fibroblast Culture Media in sterile T25 flask (with filter top), remove medium from T25 flask (the bottom of the flask has to remain a bit wet).
7. Carefully spread the skin fragments on the surface of the T25 flask.
8. Transfer flask to the incubator and leave flask for a minimum of 3 days.
9. After a minimum of 3 days, cells start growing around the skin biopsy; these cells are not yet fibroblasts, but then you know the skin piece is really attached to the bottom of the flask. When you see these cells you can carefully add some extra medium (1mL medium). If you do not see these cells yet, add only 0.5mL medium to prevent the skin pieces from starting to float.
10. Look at flask every 2-3 days. You may add additional medium until 5mL medium in total. Add only 0.5 ml medium every time very carefully. Finally, when you have added 5mL medium in total, you have to refresh the medium

every 2-3 days. Most likely, fibroblasts are then growing out of the initial cell layer.

11. If necessary, because the fibroblasts start growing only from 3-4 sites in the T25 flask, an internal trypsinization step can be performed to spread the fibroblasts over the whole T25 flask:
 - a. Add 0.5mL 2x trypsin to T25 flask
 - b. When the cells are detached, add 4.5mL medium
12. When T25 flask is completely filled with fibroblasts, transfer fibroblasts to T75 flask (0.5mL 2x trypsin + 9.5 ml medium).
13. When the T75 flask is ~70% confluent, refer to the Passaging and Freezing of Fibroblast Cells protocol.

For most experiments fibroblasts should be used between second and fifth passage. Alternatively early passage cells can be frozen and used in future experiments.

How to Harvest Myoblast Cells from CD-1 Mice

1. Sacrifice 1-5 neonatal mice by CO₂ inhalation.
2. Rinse the anterior tibialis of the left and right legs with 70% ethanol and remove with sterile scissors.
3. Place all muscle samples in a 15mL tube with 5-8mL transport media.
4. Place the 15mL tube in a foam icebox. This can be left on ice for up to 2.5h.
5. Aspirate the transport media and wash the sample with 10mL PBS 1X pH 7.2.
6. Aspirate PBS and replace with 5mL PBS.
7. Pour specimen into sterile Petri dish and mince using two sterile #10 scalpels. Repeat this till the muscle is slurry.
8. Pipette up as much of the specimen as possible and transfer to a 15mL sterile tube. Wash the plate with an additional 5mL of PBS.
9. Let the specimen settle to the bottom of the tube and aspirate off the PBS carefully.
10. Pipette 10mL PBS onto the specimen. Cap tube and shake well. Let the specimen fall to the bottom of the tube, then aspirate off the PBS.
11. Repeat steps 9+10 two more times.
12. Aspirate the PBS, add 1.6mL of the Dispase II solution, 2mL of the Collagenase IV solution and 40µl of 0.25M CaCl₂.
13. Incubate in 37°C water bath for 1 hr.
14. Triturate (pipette up and down) 10 times, try to avoid producing foam, return to water bath

for an additional 15 mins.

15. If tissue does not appear disassociated (by eye), repeat incubation and trituration.
16. Place a 100 μ m nylon cell strainer on top of a 50mL tube, pre-wet filter with PBS.
17. Pass sample through cell strainer and rinse strainer with an additional 5ml PBS.
18. Pellet cells (1500 rpm for 5 min), aspirate supernatant and re-suspend in 10ml of **Primary Culture Media**.
19. Preplate for 1.5 hrs on a standard Petri dish (non-TC coated!). This will allow contaminating fibroblasts to adhere, but myoblasts will not.
20. Transfer medium to a T75 flask and discard the Petri dish.

How to Passage Cells from CD-1 Mice

1. Before starting in sterile hood, visually check that the media is not cloudy (i.e. contaminated). Cells should be at ~70% confluency.
2. Aspirate the old culture media and wash with PBS 1X pH 7.2.
3. Aspirate PBS, and add 5mL of 0.25% Trypsin with EDTA to detach monolayer for 5-7 minutes and place in the incubator.
4. After 5 minutes, agitate (gently hit against side of table without having solution splash) and check under microscope.
5. Tilt flask, Add 20mL of respective media to inactivate T/E. Make sure to pipette slowly across the base of the flask so that all cells, will slide to the bottom.
6. Pipette the cell-media solution into a 50mL centrifuge tube and count cells using hemocytometer. Centrifuge at 1000rpm for 7 minutes.
7. Discard supernatant, and add 30 mL Primary Fibroblast Culture Media.
8. Split into 3-4 T75 flasks. Write down initials, date of creation, date of passaging, pass number, type of cell, and number of cells on flask.

To freeze cells for future culture

1. Aspirate media and wash with PBS.
2. Aspirate PBS, and add 5mL of 0.25% Trypsin with EDTA to detach monolayer for 5-7 minutes and place in the incubator.
3. Prepare freezer medium- 14mls 10% FBS, 2mls DMSO, 4mls neat FBS – total 20mls = 20% FBS, 10% DMSO. Filter.
4. -Add 1ml FM to pellet per cryo-tube. Usually split T75 into 2/3 cryo tubes. 1ml to each tube.

5. -Put in -80 freezer o/n then transfer to liquid N2.

Protocol: Seeding Myoblasts and Fibroblasts onto Ch-mesh (1:1)

1. Sterilize aluminum washers using an autoclave.
2. In the tissue culture hood, place sterile Ch-mesh samples (0.1-0.5 wt%) + the control (Avaulta Solo® Synthetic Support) in individual wells in a 6-well Cell Culture Plate, tissue culture treated, (BD Falcon™ 353046).
3. Pipette 3 mL of laminin-1 solution (50 ug/mL; Sigma) in DPBS (without Ca/Mg; pH 7.4; Mediatech). The mesh should be incubated overnight. Meanwhile, label myoblast and fibroblast cells with DiI and DiO.
4. In the tissue culture hood, remove mesh from laminin-1 solution, rinse with DPBS, and place into another sterile 6-well plate.
5. Further sterilize the mesh under UV light in a clean bench under laminar flow.
6. Soak the porous scaffolds with DMEM for 1 h.
7. Place a sterilized stainless steel washer in each well so that the maximum surface of Ch-mesh is visible in the center.
8. Trypsinize myoblasts and fibroblasts from their respective T75 flasks and count myoblast and fibroblast cells separately.
9. Collect trypsinized solutions in two separate 50mL centrifuge tubes.
10. Centrifuge both solutions (1500 rpm for 6 min).
11. Aspirate old media and add growth media at a dilution so that both primary cell strains have a density of 5×10^5 cells/ml.
12. Add 1.5 mL of the myoblast solution and 1.5 mL of the fibroblast solution to each well with the Ch-mesh and aluminum washers.

13. Place cells in incubator and replace media after 48 hrs.

Protocol: Adhesion and Proliferation Assessment

Assess cells on days 1,3 and 7. Then, aspirate culture medium and using sterile forceps remove the aluminum washers. Gently rinse with PBS and fix cells with 4% formaldehyde for 5 min. Cells are ready to be counted under microscope. Count myoblast and fibroblast cells separately.

Lab Recipes

Fibroblasts

Transport media and culture media (500 mL)

100 mL	FBS (Gibco 26140-079)
5 mL	Pen/Strep (Invitrogen 1514-122)
5 mL	Hepes (Invitrogen 15630-106)
5 mL	Sodium Pyruvate (Invitrogen 11360)
385 mL	DMEM-F12 with Glutamax (Invitrogen 31331)

Store in 4°C

Freezing media

1 mL	DMSO (Sigma D2650)
9 mL	<i>Transport media and culture media (Fibroblast)</i>

Make fresh, use immediately

MRC-5

Culture media (500 mL)

50 mL	FBS (Gibco 26140-079)
5 mL	Pen/Strep (Invitrogen 1514-122)
445 mL	DMEM low glucose (VWR 16777-126)

Store in 4°C

Maintenance media (500 mL)

100 mL	FBS (Gibco 26140-079)
5 mL	Pen/Strep (Invitrogen 1514-122)
395 mL	LF-10 Nutrient Media (Gibco 11550-043)

Store in 4°C

How to use MRC-5 conditioned media for Primary Myoblast Culture:

1. Thaw vial of MRC-5 cells, plate in T75 in 10 mL Culture Media.
2. When ~70% confluent, split 1:4, when four flasks are ~70% confluent, split 1:4 again. (total 16 flasks)
3. When 16 flasks are ~70% confluent, add 10 mL of Maintenance media to each flask and incubate overnight.
4. Remove all of the media from all flasks and pool in an autoclaved 1L bottle.
5. Pass through a 0.45 μ m (Nalgene 161-0045) filter unit and aliquot 5 mL per 15 mL centrifuge tube. Store at -20°C.
6. Replace media on MRC-5 cultures with fresh maintenance media and repeat once more.

Myoblasts

Transport media (100 mL)

10 mL FBS (Gibco 26140-079)
2 mL Pen/Strep (Invitrogen 1514-122)
88 mL F-10 Nutrient Media (Gibco 11550-043)

Store in 4°C

Collagenase 4 (Worthington Chemical LS004212)

Re-suspend 100 mg in 25 mL sterile PBS,
Freeze 2 mL aliquots (Store in -20°C)

Dispase II (Roche 10 295 825 001)

Freeze 2 mL aliquots (Store in -20°C)

Trypsin, 0.25% (1X) with EDTA (Gibco 25200-056)

Dilute with PBS to make 0.1% stock.
Freeze in 4 mL aliquots (Store in -20°C)

bFGF stock (25 ng/μL)

Add 1 mL sterile PBS to the 25 μg vial.
Freeze 50 μL aliquots (Store in -20°C)

Dexamethasone stock

0.2M CaCl₂

Maintenance media (200 mL)

40 mL FBS (Gibco 26140-079)
2 mL Pen/Strep (Invitrogen 1514-122)
158 mL F-10 Nutrient Media (Gibco 11550-043)

Filter all ingredients through 0.22μm
filter unit (Corning 430767) & store in 4°C

Primary culture media (10 mL)

5 mL Maintenance media with bFGF
5 mL MRC-5 conditioned-media

Just before use, add:

1. 4 μL per 10 mL of bFGF
2. 10 μl per 10 mL of dexamethasone

Protocol: Chitosan Mesh Preparation

Step 1: Take two sets of forceps, autoclave them and place them in two separate bags.

Step 2: Use the precision balance to measure the desired amount of Chitosan (High Molecular Weight) and add it to the complementary amount of distilled H₂O

For 1% Chitosan-concentration, measure 1 g Ch, and add to 99 ml distilled H₂O. For 0.5% Chitosan-concentration, measure 0.5 g Ch, and add to 99.5 mL distilled H₂O. Etc.

Step 3: Insert a clean magnetic stir bar and dissolve overnight on the stirring plate in 1% (v/v) acetic acid solution until a clear gel is obtained (about 24 hours). Keep the beaker covered with Parafilm.

Keep consistent with the volume used in Step 2. To clarify, in the above examples, use 1 mL acetic acid with 99 mL distilled H₂O.

Step 4: In the sterile hood, sterilize this solution using Filter Units (Nalgene 568; 250mL Capacity, MF75™ Series). This solution can be stored for up to 30 days. Make sure to write your name, creation date, and expiration date in permanent marker on the bottle. Store this solution in the chemical cabinet. Place a magnetic stir bar in bleach. Remove all of the bleach with a KimWipe when you are ready for Step 7.

Step 5: Cut Bard® polypropylene mesh into 1.2 x 1.2 cm squares. Weigh the sample.

Step 6: Harrick Plasma Cleaner Instructions

1. Turn on lower and upper power switches.
2. Chamber is under vacuum. Bleed air into the chamber by opening needle valve 1/2 turn. When door can be opened, close needle valve.
3. Put samples in open petri dish and place in chamber.
4. Ensure "O" ring is clean and close door.
5. Turn on the vacuum pump switch on the front of the Plasma Cleaner while holding the door shut for the first few seconds.
6. Pump down to ~500 mtorr (green range of pressure where the plasma is the brightest pink color)
7. Select RF level HI by *gently* turning the knob. This will start plasma generation. Coat sample with plasma for 32 seconds.
8. Turn off RF.
9. Turn off vacuum.
10. Vent the chamber to atmosphere, open door, and close needle valve.
11. Using rubber-tipped forceps, flip the sample over so the uncoated side is facing up on the petri dish. Repeat steps D-J.
12. When finished, close door, and while holding door, start vacuum and allow pumping down to 300 mtorr.

13. Turn off vacuum and Plasma Cleaner power switches.

Step 7: Immediately after removing the mesh from the Plasma Cleaner, insert the mesh and stir bar into a sterile bottle containing the filtered Chitosan solution from Step 4. Use rubber tipped forceps and make this transfer as quick as possible to ensure maximum charge retention. Close the cap tightly and place on top of the stirring plate. Leave this overnight.

Step 8: Sterilize in UV (in the bio-hood) for 20 minutes, placed at an angle on a petri dish so both sides are exposed. *Or: In the sterile hood and using the first pair of sterile forceps for handling the mesh, remove the mesh from the filtered chitosan solution. Sterilize this mesh by letting it soak in a petri dish in 70% ethanol for ten minutes and aspirating off the aqueous solution. Repeat 3 times. Let this dry in the sterile hood for an hour with the ventilation on. After an hour, if the mesh when handled is still not dry, then let it sit for another hour in the sterile hood till all ethanol has evaporated.*

Step 9: In the sterile hood and using the second set of sterile forceps, remove the mesh and put it into a 15 mL tube. Replace the cap, and place in the lyophilizer at -40°C for 24 hours. Label the 15 mL tubes with your name, Chitosan concentration, and the creation date.

Step 10: Lyophilizer Instructions

- 1. Log onto NBTC Computer**
- 2. Loosen the caps of the 15 mL tubes containing the coated meshes. Do not make these too loose, however, or the vacuum in the lyophilizer will dislodge them.**
- 3. Place them in a glass container with no nicks on the glass and a solid lid. Make sure the black lid is *tightly* sealed. Carefully put the bent glass tube leading out of the lid into the machine.**
- 4. Place the glass container into a larger styrofoam container. Pour liquid nitrogen in the styrofoam box - this ensures the sample is kept frozen for the first two hours.**
- 5. *Slowly* turn the flat knob on the machine clockwise until you reach the highlighted part. This will open up the vacuum valve. If there is a problem with attaining a vacuum using the current setup, use parafilm to seal any leaks.**
- 6. Label glass container with Name, Date, Contents of Container, Net ID. Log on to NBTC computer. Leave samples for 24 hours.**
- 7. After 24 hours, retrieve samples and tighten all lids. Log off the NBTC computer.**

Step 11: Remove samples from lyophilizer. Weigh the sample in a pre-weighted 15 mL tube.

APPENDIX II: rat model protocols

Location: Weill Surgical Suite

Protocol	Equipment or material required
Prior to Euthanizing:	
<ol style="list-style-type: none"> 1. Collect dry ice in Styrofoam box 2. Bring camera for pictures 3. Fill 15ml centrifuge tubes sent to histology with formalin using plastic pipette 	<i>Styrofoam box</i> <i>Plastic pipette</i> <i>15ml centrifuge tubes</i> <i>10% formalin</i>
Euthanize	
<ol style="list-style-type: none"> 1. Remove top of cage and replace with clear disc 2. Attach tube and turn pink knob. Allow rat to remain in cage for 3 minutes after in stops breathing 	
Necropsy	
<ol style="list-style-type: none"> 1. Remove rat and place on blue drape 2. Make midline incision and expose abdomen with both mesh samples. Using camera, take image. 3. Excise mesh sample (one at a time) and label appropriate centrifuge tubes 4. Place sample on corkboard and pin down sample. Using camera, take image. 5. Use dogbone punch to collect tensile testing sample. Using camera, take image of process. Place sample in centrifuge tube and in dry ice Styrofoam box. 6. Use remaining tissue for histology, place in formalin-filled centrifuge tubes. 7. Wrap up animal in black trash bag and put in necropsy room. 8. Wash down corkboard, forceps and scissors. Throw away other items. 	<i>Clean forceps and scissors</i> <i>Blue drape</i> <i>Corkboard and pins</i> <i>Camera</i> <i>Black marker for labeling</i> <i>Dogbone punch</i>

Protocol	Equipment or material required
<p>F-canister</p> <ol style="list-style-type: none"> 4. Fill in isoflurane so that it is in-between the line on the vaporizer. 5. Check to make sure F-canister did not gain more than 50 grams, replace if over 50 grams. 6. Turn O2 knob clockwise (green knob). Set at 0.8L 7. The top knob is for iso. Push down and turn the knob. Set at 2. 	
<p>Rat Handling</p> <ol style="list-style-type: none"> 1. Turn on heated table. 2. Tape blue drape down to heated table. 3. On surgical table, inject meloxicam (dose will depend on size of rat - 1ml/250g rat) into scruff of rat. 4. Hold the rat by the base of its tail and place in the induction box. Snap to close. Start iso at 3. 	<p><i>Heating pads</i> <i>Sterile blue drapes (cut to size)</i> <i>Meloxicam bottle</i> <i>Needle Syringes</i></p>
<p>Anaesthetize</p> <ol style="list-style-type: none"> 1. Turn on iso and O2. 2. Once rat is sedated, place rat on blue drape, and put nose in nose cone. 3. Use clippers to shave belly – keep swab flat with skin. Remove hair with handheld vacuum. 4. Pinch toes hard – look for movement. 5. Tape individual legs to prevent moving. Set iso at 2. 6. Start swiping down the center of the skin patch with betadine and move to the outside. Use 5 swab sheets. 7. Take one swab, soak in betadine, and place on abdomen. Pinch toes hard to assess anesthesia depth. Set iso at 1.5-2 depending on the anesthesia depth. 8. Administer small amount of eye lube to eyes of rat. 9. Place sterile blue drape on top of rat with hole made for surgery. 10. Keep monitoring the anesthesia depth by toe pinching every 5-10 minutes during anesthesia. Be careful not to touch the top side of the blue pad and keep your hands under the pad while trying to pinch the toe. 11. Reduce iso to 1 when subcuticular sutures are being placed and gradually decrease to 0 when the suturing is complete. 	<p><i>Wahl clippers</i> <i>Betadine surgical scrub</i> <i>Porous tape</i> <i>Portable Handheld vacuum</i></p>
<p>SURGERY</p>	<p><i>Adjustable chair (Gao room)</i> <i>4-0 prolene sutures</i> <i>4-0 vicryl sutures</i></p>



Post-surgery

1. Clean wound with hydrogen peroxide; use vetbond if necessary.
2. Place tools in Bead sterilizer if required for more surgeries.
3. If finished with surgery, weigh F-canister and label.
4. For recovery, place the animal in an empty cage (no bedding) with an activated hand warmer placed underneath the cage. When the animal starts to ambulate, place it back in its home cage.

*Hydrogen peroxide
Vetbond
Bead sterilizer*

Location: Bonassar's Lab (Enduratec Station)

Protocol	Equipment or material required
<p>Prepping the sample:</p> <ol style="list-style-type: none"> 8. Place sample in 15 ml centrifuge tube in -80 freezer 9. When ready to use, equilibrate sample in water bath for 10 min prior to testing sample 	<p><i>15mL centrifuge tube</i> <i>Water bath</i></p>
<p>Prepping the machine:</p> <ol style="list-style-type: none"> 3. Remove compression device using allen wrench 4. Turn on load cell box (top machine) and equipment that controls movement of machine (bottom) 5. Use 50 lb load cell (nub on top), then screw in the black knob at the bottom 6. Screw clams into load cell (does not need to be tight) 7. Only turn the black knob on the base NOT the load cell (it will kink) 8. Adjust height between clamps with the allen wrench 	
<p>Running the software:</p> <ol style="list-style-type: none"> 9. Turn on both control boxes (switches on back) 10. Open WinTest > Program Files 11. Open My Computer > C:\ > Program Files > Enduratec > Natasha_1000g 12. (Blue Line – disp of top actuator, Green line – force) 13. Define waveform – delete everything and program system using Block Type <ol style="list-style-type: none"> a. Precondition with 10 sinusoidal cycles at 0.167 mm/sec -1 mm peaks (half sine, sine) b. Load-to-failure test performed at 0.15 mm/sec (ramp) 14. Timed data <ol style="list-style-type: none"> a. Scan time (total time) = 276 sec b. Scan Points = 552 15. File Info > Browse > Natasha folder on desktop > NAME FILE 16. Local > Select high (information flowing b/w computer and control box) 17. Home (Position Axial -•-) > Set to -4.8 18. Setup > Channels > Filters tab > 10 Hz load 	

and displacement (frequency times 2)	
Begin testing:	
<ol style="list-style-type: none"> 1. Using sandpaper capped around ends, insert sample into fixture (top clamp first). Push black knob up to move bottom clamp. To lock bottom clamp, use tool with blue handle. Take photo. 2. To ensure that samples are tested consistently, an aspect ratio (length to width ratio) of 3 must be maintained for all samples 3. Record all measurements in lab notebook (thickness, width, and length) 4. Allow 5 min to equilibrate, squirt saline if necessary 5. Setup > Channel: Load > Tare (check to see that Load equilibrates to 0) 6. Timed data > File Info > Select file (check to make sure you have highlighted the correct load) > Start 7. Run button > Zero Start 8. Take photo as load-to-failure is happening. Write in lab notebook where failure occurred 	<i>Sandpaper</i> <i>Saline solution</i> <i>Calibrated calipers</i> <i>Camera</i>

References

1. MacLennan A, Taylor A. The prevalence of pelvic floor disorders and their relationship to gender, age, parity and mode of delivery. *J. Obstet. Gynaecol.* (Lahore). **107**, 1460, 2000;
2. Sung V, Hampton B. Epidemiology of Pelvic Floor Dysfunction. *Obstet. Gynecol. Clin. North Am.* **36**, 421, 2009;
3. Abramowitch SD, Feola A, Jallah Z, Moalli P a. Tissue mechanics, animal models, and pelvic organ prolapse: a review. *Eur. J. Obstet. Gynecol. Reprod. Biol.* **144 Suppl** , S146, 2009;
4. Subak LL, Waetjen LE, van den Eeden S, Thom DH, Vittinghoff E, Brown JS. Cost of pelvic organ prolapse surgery in the United States. *Obstet. Gynecol.* **98**(4), 646, 2001;
5. Luber KM, Boero S, Choe JY. The demographics of pelvic floor disorders: Current observations and future projections. *Am. J. Obstet. Gynecol.* **184**(7), 1496, 2001;
6. Herschorn S. Female pelvic floor anatomy: the pelvic floor, supporting structures, and pelvic organs. *Rev. Urol.* **6 Suppl 5**, S2, 2004;
7. Winters JC, Togami JM, Chermansky C. Chapter 72: Vaginal and Abdominal Reconstructive Surgery for Pelvic Organ Prolapse. *Campbell-Walsh Urol.* 10th Ed. Rev. Tenth Edit. Elsevier Inc.; p. 2069–114, 2005.

8. Ashton-Miller JA, DeLancey JOL. On the Biomechanics of Vaginal Birth and Common Sequelae. *Annu. Rev. Biomed. Eng. Annual Reviews*; **11**, 163, 2009;
9. Colborn GL, Jr. RMR, Skandalakis JE. Chapter 28: Pelvis and Perineum. *Skandalakis' Surg. Anat.* 2006.
10. Jelovsek JE, Maher C, Barber MD. Pelvic organ prolapse. *Lancet*. **369**(9566), 1027, 2007;
11. Dietz HP. Levator function before and after childbirth. *Aust. N. Z. J. Obstet. Gynaecol.* **44**(1), 19, 2004;
12. Ashton-Miller JA, DeLancey JOL. Functional anatomy of the female pelvic floor. *Ann. N. Y. Acad. Sci.* **1101**, 266, 2007;
13. DeLancey JOL, Morgan DM, Fenner DE, Kearney R, Guire K, Miller JM, et al. Comparison of levator ani muscle defects and function in women with and without pelvic organ prolapse. *Obstet. & Gynecol. Surv. Lippincott Williams & Wilkins*; **62**(6), 374, 2007;
14. Hendrix SL, Clark A, Nygaard I, Aragaki A, Barnabei V, McTiernan A. Pelvic organ prolapse in the women's health initiative: Gravity and gravidity. *Am. J. Obstet. Gynecol.* **186**(6), 1160, 2002;
15. Handa VL, Harvey L, Cundiff GW, Siddique S a, Kjerulff KH. Sexual function among women with urinary incontinence and pelvic organ prolapse. *Am. J. Obstet. Gynecol.* **191**(3), 751, 2004;

16. Nygaard I, Barber MD, Burgio KL, Kenton K, Meikle S, Schaffer J, et al. Prevalence of symptomatic pelvic floor disorders in US women. *JAMA*. **300**(11), 1311, 2008;
17. Lowder JL, Debes KM, Moon DK, Howden N, Abramowitch SD, Moalli P a. Biomechanical adaptations of the rat vagina and supportive tissues in pregnancy to accommodate delivery. *Obstet. Gynecol.* **109**(1), 136, 2007;
18. Olsen a L, Smith VJ, Bergstrom JO, Colling JC, Clark a L. Epidemiology of surgically managed pelvic organ prolapse and urinary incontinence. *Obstet. Gynecol.* **89**(4), 501, 1997;
19. Keys T, Campeau L, Badlani G. Synthetic mesh in the surgical repair of pelvic organ prolapse: current status and future directions. *Urology*. Elsevier Inc.; **80**(2), 237, 2012;
20. McCulloch P, Altman DG, Campbell WB, Flum DR, Glasziou P, Marshall JC, et al. No surgical innovation without evaluation: the IDEAL recommendations. *Lancet*. Elsevier Ltd; **374**(9695), 1105, 2009;
21. Altman D, Väyrynen T, Engh ME, Axelsen S, Falconer C. Anterior colporrhaphy versus transvaginal mesh for pelvic-organ prolapse. *N. Engl. J. Med.* **364**(19), 1826, 2011;
22. Menefee S a, Dyer KY, Lukacz ES, Simsiman AJ, Luber KM, Nguyen JN. Colporrhaphy compared with mesh or graft-reinforced vaginal paravaginal repair

- for anterior vaginal wall prolapse: a randomized controlled trial. *Obstet. Gynecol.* **118**(6), 1337, 2011;
23. Stanford EJ, Cassidenti a, Moen MD. Traditional native tissue versus mesh-augmented pelvic organ prolapse repairs: providing an accurate interpretation of current literature. *Int. Urogynecol. J.* **23**(1), 19, 2012;
 24. Jeffery S, de Jong P. MESH, GRAFTS AND KITS IN PELVIC ORGAN PROLAPSE SURGERY: WHERE ARE WE NOW ? *South Africa Urogynaecology Rev.* **61**, 13, 2009;
 25. Gualtieri M, Zhang Y, Candiotti K, Yavagal S, Medina CA, Takacs P. The effect of biological and synthetic meshes on vaginal smooth muscle cell proliferation. *Neurourol. Urodyn. Wiley Online Library*; (December 2010), 1, 2011;
 26. Elsabee MZ, Abdou ES, Nagy KS a., Eweis M. Surface modification of polypropylene films by chitosan and chitosan/pectin multilayer. *Carbohydr. Polym.* **71**(2), 187, 2008;
 27. Dwyer PL. Evolution of biological and synthetic grafts in reconstructive pelvic surgery. *Int. Urogynecol. J. Pelvic Floor Dysfunct.* **17 Suppl 1**, S10, 2006;
 28. Jones K a, Feola A, Meyn L, Abramowitch SD, Moalli P a. Tensile properties of commonly used prolapse meshes. *Int. Urogynecol. J. Pelvic Floor Dysfunct.* **20**(7), 847, 2009;

29. De Tayrac R, Devoldere G, Renaudie J, Villard P, Guilbaud O, Eglin G. Prolapse repair by vaginal route using a new protected low-weight polypropylene mesh: 1-year functional and anatomical outcome in a prospective multicentre study. *Int. Urogynecol. J. Pelvic Floor Dysfunct.* **18**(3), 251, 2007;
30. Boyles SH, Weber AM, Meyn L. Procedures for urinary incontinence in the United States, 1979-1997. *Am. J. Obstet. Gynecol.* **189**(1), 70, 2003;
31. Brown JS, Waetjen LE, Subak LL, Thom DH, Van Den Eeden S, Vittinghoff E. Pelvic organ prolapse surgery in the United States, 1997. *Am. J. Obstet. Gynecol.* **186**(4), 712, 2002;
32. Van Geelen JM, Dwyer PL. Where to for pelvic organ prolapse treatment after the FDA pronouncements? Reply to Pelikan. *Int. Urogynecol. J.* **24**(11), 1991, 2013;
33. Menchen LC, Wein AJ, Smith AL. An appraisal of the Food and Drug Administration warning on urogynecologic surgical mesh. *Curr. Urol. Rep.* **13**(3), 231, 2012;
34. Patel H, Ostergard DR, Sternschuss G. Polypropylene mesh and the host response. *Int. Urogynecol. J.* **23**(6), 669, 2012;
35. Abdel-Fattah M, Familusi A, Fielding S, Ford J, Bhattacharya S. Primary and repeat surgical treatment for female pelvic organ prolapse and incontinence in parous women in the UK: a register linkage study. *BMJ Open.* **1**(2), e000206, 2011;

36. Shepherd JP, Feola AJ, Abramowitch SD, Moalli P a. Uniaxial biomechanical properties of seven different vaginally implanted meshes for pelvic organ prolapse. *Int. Urogynecol. J.* **23**(5), 613, 2012;
37. Cassar K, Munro a. Surgical treatment of incisional hernia. *Br. J. Surg.* **89**(5), 534, 2002;
38. Paulo NM, de Brito e Silva MS, Moraes AM, Rodrigues AP, de Menezes LB, Miguel MP, et al. Use of chitosan membrane associated with polypropylene mesh to prevent peritoneal adhesion in rats. *J. Biomed. Mater. Res. B. Appl. Biomater.* **91**(1), 221, 2009;
39. Abed A, Deval B, Assoul N, Bataille I, Portes P, Louedec L, et al. A biocompatible polysaccharide hydrogel-embedded polypropylene mesh for enhanced tissue integration in rats. *Tissue Eng. Part A.* **14**(4), 519, 2008;
40. Gonzalez R, Fugate K, McClusky D, Ritter EM, Lederman A, Dillehay D, et al. Relationship between tissue ingrowth and mesh contraction. *World J. Surg.* **29**(8), 1038, 2005;
41. Brizzolara S. Risk of mesh erosion with sacral colpopexy and concurrent hysterectomy. *Obstet. Gynecol.* **102**(2), 306, 2003;
42. Hjort H, Mathisen T, Alves a, Clermont G, Boutrand JP. Three-year results from a preclinical implantation study of a long-term resorbable surgical mesh with time-dependent mechanical characteristics. *Hernia.* **16**(2), 191, 2012;

43. Iannitti D a, Hope WW, Tsikitis V. Strength of tissue attachment to composite and ePTFE grafts after ventral hernia repair. *JLS*. **11**(4), 415, 2007;
44. Sanders DL, Kingsnorth AN. Prosthetic mesh materials used in hernia surgery. *Expert Rev. Med. Devices*. **9**(2), 159, 2012;
45. LeBlanc K a, Bellanger D, Rhynes K V, Baker DG, Stout RW. Tissue attachment strength of prosthetic meshes used in ventral and incisional hernia repair. A study in the New Zealand White rabbit adhesion model. *Surg. Endosc*. **16**(11), 1542, 2002;
46. Bazi T, Ammouri AH, Hamade RF. On the relevance of uniaxial tensile testing of urogynecological prostheses: the effect of displacement rate. *Int. Urogynecol. J*. **24**(1), 161, 2013;
47. Moalli P a, Howden NS, Lowder JL, Navarro J, Debes KM, Abramowitch SD, et al. A rat model to study the structural properties of the vagina and its supportive tissues. *Am. J. Obstet. Gynecol*. **192**(1), 80, 2005;
48. VandeVord P, Matthew H, DeSilva S, Mayton L, Wu B, Wooley P. Evaluation of the biocompatibility of a chitosan scaffold in mice. *J. Biomed. Mater. Res*. **59**(3), 585, 2002;
49. Machingal MA, Corona BT, Walters TJ, Kesireddy V, Koval CN, Dannahower A, et al. A Tissue-Engineered Muscle Repair Construct for Functional Restoration of an Irrecoverable Muscle Injury in a Murine Model. *Tissue Eng. Part A. Mary Ann*

- Liebert, Inc. 140 Huguenot Street, 3rd Floor New Rochelle, NY 10801 USA; 17(17-18), 2291, 2011;
50. Hernández-Gascón B, Peña E, Pascual G, Rodríguez M, Bellón JM, Calvo B. Long-term anisotropic mechanical response of surgical meshes used to repair abdominal wall defects. *J. Mech. Behav. Biomed. Mater. Elsevier Ltd*; 5(1), 257, 2012;
 51. Bellón JM, Buján J, Contreras L, Hernando a. Integration of biomaterials implanted into abdominal wall: process of scar formation and macrophage response. *Biomaterials*. 16(5), 381, 1995;
 52. Huber A, Boruch A V, Nieponice A, Jiang H, Medberry C, Badylak SF. Histopathologic host response to polypropylene-based surgical mesh materials in a rat abdominal wall defect model. *J. Biomed. Mater. Res. B. Appl. Biomater.* 100(3), 709, 2012;
 53. Zogbi L, Portella a O V, Trindade MRM, Trindade EN. Retraction and fibroplasia in a polypropylene prosthesis: experimental study in rats. *Hernia*. 14(3), 291, 2010;
 54. Krause H, Goh J. Sheep and rabbit genital tracts and abdominal wall as an implantation model for the study of surgical mesh. *J. Obstet. Gynaecol. Res.* 35(2), 219, 2009;
 55. Matthews B. Assessment of adhesion formation to intra-abdominal polypropylene mesh and polytetrafluoroethylene mesh. *J. Surg. Res.* 114(2), 126, 2003;

56. Brown BN, Londono R, Tottey S, Zhang L, Kukla K a, Wolf MT, et al. Macrophage phenotype as a predictor of constructive remodeling following the implantation of biologically derived surgical mesh materials. *Acta Biomater.* **8**(3), 978, 2012;
57. Altinel Y, Öztürk E, Özkaya G, Akyıldız EÜ, Ulcay Y, Özgüç H. The effect of a chitosan coating on the adhesive potential and tensile strength of polypropylene meshes. *Hernia.* **16**(6), 709, 2012;
58. Sergent F, Desilles N, Lacoume Y, Bunel C, Marie J-P, Marpeau L. Experimental biomechanical evaluation of polypropylene prostheses used in pelvic organ prolapse surgery. *Int. Urogynecol. J. Pelvic Floor Dysfunct.* 597, 2009;
59. De Tayrac R, Alves A, Thérin M. Collagen-coated vs noncoated low-weight polypropylene meshes in a sheep model for vaginal surgery. A pilot study. *Int. Urogynecol. J. Pelvic Floor Dysfunct.* **18**(5), 513, 2007;
60. Kohli N, Miklos JR. Use of synthetic mesh and donor grafts in gynecologic surgery. *Curr. Womens. Health Rep.* **1**(1), 53, 2001;
61. Cervigni M, Natale F, La Penna C, Saltari M, Padoa A, Agostini M. Collagen-coated polypropylene mesh in vaginal prolapse surgery: an observational study. *Eur. J. Obstet. Gynecol. Reprod. Biol.* Elsevier Ireland Ltd; **1**, 2011;
62. Brown BN, Valentin JE, Stewart-Akers AM, McCabe GP, Badylak SF. Macrophage phenotype and remodeling outcomes in response to biologic scaffolds with and without a cellular component. *Biomaterials.* Elsevier Ltd; **30**(8), 1482, 2009;

63. Valentin JE, Turner NJ, Gilbert TW, Badylak SF. Functional skeletal muscle formation with a biologic scaffold. *Biomaterials*. Elsevier Ltd; **31**(29), 7475, 2010;
64. Cakmak A, Cirpanli Y, Bilensoy E, Yorganci K, Caliş S, Saribaş Z, et al. Antibacterial activity of triclosan chitosan coated graft on hernia graft infection model. *Int. J. Pharm.* **381**(2), 214, 2009;
65. Funakoshi T, Majima T, Iwasaki N, Yamane S, Masuko T, Minami A, et al. Novel chitosan-based hyaluronan hybrid polymer fibers as a scaffold in ligament tissue engineering. *J. Biomed. Mater. Res. A.* **74**(3), 338, 2005;
66. Stekelenburg M, Rutten MCM, Snoeckx LHEH, Baaijens FPT. Dynamic straining combined with fibrin gel cell seeding improves strength of tissue-engineered small-diameter vascular grafts. *Tissue Eng. Part A.* **15**(5), 1081, 2009;
67. Chen G, Ushida T, Tateishi T. A hybrid network of synthetic polymer mesh and collagen sponge. *Chem. Commun.* **360**(16), 1505, 2000;
68. Hill E, Boontheekul T, Mooney DJ. Designing scaffolds to enhance transplanted myoblast survival and migration. *Tissue Eng.* **12**(5), 1295, 2006;
69. Bartone F, Adickes E. Chitosan: Effects on Wound Healing in Urogenital Tissue: Preliminary Report. *J. Urol.* **140**(5 Pt 2), 1134, 1988;
70. Tangsadthakun C, Kanokpanont S, Sanchavanakit N, Banaprasert T, Damrongsakkul S. Properties of collagen/ chitosan scaffolds for skin tissue engineering. *J. Met. Mater. Miner.* **16**(1), 37, 2006;

71. Muzzarelli R a. a. Chitins and chitosans for the repair of wounded skin, nerve, cartilage and bone. *Carbohydr. Polym. Elsevier Ltd*; **76**(2), 167, 2009;
72. Kim I-Y, Seo S-J, Moon H-S, Yoo M-K, Park I-Y, Kim B-C, et al. Chitosan and its derivatives for tissue engineering applications. *Biotechnol. Adv.* **26**(1), 1, 2008;
73. Chung LY, Schmidt RJ, Hamlyn PF, Sagar BF, Andrews a M, Turner TD. Biocompatibility of potential wound management products: fungal mycelia as a source of chitin/ chitosan and their effect on the proliferation of human F1000 fibroblasts in culture. *J. Biomed. Mater. Res.* **28**(4), 463, 1994;
74. Zakhem E, Raghavan S, Gilmont RR, Bitar KN. Chitosan-based scaffolds for the support of smooth muscle constructs in intestinal tissue engineering. *Biomaterials.* **33**, 4810, 2012;
75. Madden LR, Mortisen DJ, Sussman EM, Dupras SK, Fugate J a, Cuy JL, et al. Proangiogenic scaffolds as functional templates for cardiac tissue engineering. *Proc. Natl. Acad. Sci. U. S. A.* **107**(34), 15211, 2010;
76. Pierce LM, Grunlan M a, Hou Y, Baumann SS, Kuehl TJ, Muir TW. Biomechanical properties of synthetic and biologic graft materials following long-term implantation in the rabbit abdomen and vagina. *Am. J. Obstet. Gynecol. Mosby, Inc.*; **200**(5), 549.e1, 2009;
77. Ayubi FS, Armstrong PJ, Mattia MS, Parker DM. Abdominal wall hernia repair: a comparison of Permacol and Surgisis grafts in a rat hernia model. *Hernia.* **12**(4), 373, 2008;

78. Kilic D, Agalar C, Ozturk E, Denkbaz EB, Cime A, Agalar F. Antimicrobial activity of cefazolin-impregnated mesh grafts. *ANZ J. Surg.* **77**(4), 256, 2007;
79. Cosson M, Debodinance P, Boukerrou M, Chauvet M, Lobry P, Crepin G, et al. Mechanical properties of synthetic implants used in the repair of prolapse and urinary incontinence in women: which is the ideal material? *Int. Urogynecol. J. Springer*; **14**(3), 169, 2003;
80. Goldstein HS. Selecting the right mesh. *Hernia.* **3**(1), 23, 1999;
81. Gobin AS, Butler CE, Mathur AB. Repair and regeneration of the abdominal wall musculofascial defect using silk fibroin-chitosan blend. *Tissue Eng. Mary Ann Liebert, Inc. 2 Madison Avenue Larchmont, NY 10538 USA*; **12**(12), 3383, 2006;
82. Wang X. A Comparison of Chitosan and Collagen Sponges as Hemostatic Dressings. *J. Bioact. Compat. Polym.* **21**(1), 39, 2006;
83. Ławniczak P, Grobelski B, Pasięka Z. Properties comparison of intraperitoneal hernia meshes in reconstruction of the abdominal wall: animal model study. *Pol. Przegl. Chir.* **83**(1), 19, 2011;
84. Snowden J. Preparing Primary Cultures from Muscle Biopsy Specimens [Internet]. Univ. Rochester Med. Cent. Website. p. 5–7, [cited 2010 Aug 11]. Available from: <http://www.urmc.rochester.edu/fields-center/protocols/myoblast-cell-cultures.cfm>

85. Tsai W, Chu C, Chiu S, Yao J. In vitro quantitative study of newly made antibacterial braided nylon sutures. *Surg Gynecol Obs.* **165**, 207, 1987;
86. Sewell W, Wiland J, Craver B. A new method of comparing sutures of ovine catgut with sutures of bovine catgut in three species. *Surg. Gynecol. Obstet.* **100**, 483, 1955;
87. Wright WE, Sassoon D a, Lin VK. Myogenin, a factor regulating myogenesis, has a domain homologous to MyoD. *Cell.* **56**(4), 607, 1989;
88. Voyles CR, Richardson JD, Bland KI, Tobin GR, Flint LM, Polk HC. Emergency abdominal wall reconstruction with polypropylene mesh: short-term benefits versus long-term complications. *Ann. Surg.* **194**(2), 219, 1981;
89. Neumann T, Hauschka SD, Sanders JE. Tissue engineering of skeletal muscle using polymer fiber arrays. *Tissue Eng.* **9**(5), 995, 2003;
90. Chen G, Sato T, Ohgushi H, Ushida T, Tateishi T, Tanaka J. Culturing of skin fibroblasts in a thin PLGA-collagen hybrid mesh. *Biomaterials.* **26**(15), 2559, 2005;
91. Diegelmann RF, Dunn JD, Lindblad WJ, Cohen IK. Analysis of the effects of chitosan on inflammation, angiogenesis, fibroplasia, and collagen deposition in polyvinyl alcohol sponge implants in rat wounds. *Wound Repair Regen.* **4**(1), 48, 1996;

92. Mokarram N, Merchant A, Mukhatyar V, Patel G, Bellamkonda R V. Effect of modulating macrophage phenotype on peripheral nerve repair. *Biomaterials*. Elsevier Ltd; **33**(34), 8793, 2012;
93. Rao A, Gibon E, Ma T, Yao Z, Smith R, Goodman S. Revision joint replacement, wear particles, and macrophage polarization. *Acta Biomater*. Acta Materialia Inc.; **8**(7), 2815, 2012;
94. Ilie C, Chancellor M. Female Urology-Future and Present. *Rev. Urol*. **12**(2), 2009, 2010;
95. Konstantinovic M, Ozog Y, Spelzini F. Biomechanical findings in rats undergoing fascial reconstruction with graft materials suggested as an alternative to polypropylene. *Neurourol. Urodyn*. **493**(April 2009), 488, 2010;
96. Moalli P a, Papas N, Menefee S, Albo M, Meyn L, Abramowitch SD. Tensile properties of five commonly used mid-urethral slings relative to the TVT. *Int. Urogynecol. J. Pelvic Floor Dysfunct*. **19**(5), 655, 2008;
97. Dietz HP, Vancaillie P, Svehla M, Walsh W, Steensma a B, Vancaillie TG. Mechanical properties of urogynecologic implant materials. *Int. Urogynecol. J. Pelvic Floor Dysfunct*. **14**(4), 239, 2003;
98. Papadimitriou J, Petros PEP. Re: Biocompatible properties of surgical mesh using an animal model. *Aust. New Zeal. J. Obstet. Gynaecol*. **46**(4), 368, 2006;

99. Hernández-Gascón B, Peña E, Melero H, Pascual G, Doblaré M, Ginebra MP, et al. Mechanical behaviour of synthetic surgical meshes: finite element simulation of the herniated abdominal wall. *Acta Biomater.* 7(11), 3905, 2011;
100. Maher C, Baessler K, Glazener C, Adams E, Hagen S. Surgical management of pelvic organ prolapse in women. *Cochrane Collab.* p. 1–135, 2007.
101. Junge K, Klinge U, Rosch R, Lynen P, Binnebösel M, Conze J, et al. Improved collagen type I/III ratio at the interface of gentamicin-supplemented polyvinylidene fluoride mesh materials. *Langenbecks. Arch. Surg.* 392(4), 465, 2007;
102. Jonsson Funk M, Edenfield AL, Pate V, Visco AG, Weidner AC, Wu JM. Trends in use of surgical mesh for pelvic organ prolapse. *Am. J. Obstet. Gynecol.* 208(1), 79.e1, 2013;
103. Huebner M, Hsu Y, Fenner DE. The use of graft materials in vaginal pelvic floor surgery. *Int. J. Gynaecol. Obstet.* 92(3), 279, 2006;
104. Birk D, Mayne R. Localization of collagen types I, III and V during tendon development. Changes in collagen types I and III are correlated with changes in fibril diameter. *Eur. J. Cell Biol.* 72, 352, 1997;
105. Friedman D, Boyd C, MacKenzie J, Norton P, Olson R, Deak S. Regulation of Collagen Gene Expression in Keloids and Hypertrophic Scars. *J. Surg.* 55, 214, 1993;

106. Henkel W, Glanville R. Covalent Crosslinking between Molecules of Type I and Type III Collagen. *Eur. J.* **213**, 205, 1982;
107. Madden JW, Peacock EE. Studies on the biology of collagen during wound healing. *Plast. Reconstr. Surg.* **51**(2), 235, 1973;
108. Junge K, Rosch R, Anurov M, Titkova S, Ottinger a, Klinge U, et al. Modification of collagen formation using supplemented mesh materials. *Hernia.* **10**(6), 492, 2006;
109. Pauschinger M, Knopf D, Petschauer S, Doerner a., Poller W, Schwimmbeck PL, et al. Dilated Cardiomyopathy Is Associated With Significant Changes in Collagen Type I/III ratio. *Circulation.* **99**(21), 2750, 1999;
110. Klinge U, Klosterhalfen B, Müller M, Anurov M, Ottinger a, Schumpelick V. Influence of polyglactin-coating on functional and morphological parameters of polypropylene-mesh modifications for abdominal wall repair. *Biomaterials.* **20**(7), 613, 1999;
111. Junge K, Klinge U, Rosch R, Mertens PR, Kirch J, Klosterhalfen B, et al. Decreased collagen type I/III ratio in patients with recurring hernia after implantation of alloplastic prostheses. *Langenbecks. Arch. Surg.* **389**(1), 17, 2004;
112. Klinge U, Si Z, Zheng H. Abnormal Collagen I to III Distribution in the Skin of Patients with Incisional Hernia. *Eur. Surg.* **32**, 43, 2000;

113. Biagini G, Bertani a, Muzzarelli R, Damadei a, DiBenedetto G, Belligolli a, et al. Wound management with N-carboxybutyl chitosan. *Biomaterials*. **12**(3), 281, 1991;
114. Udpa N, Iyer SR, Rajoria R, Valentine H, Breyer KE, Singh B, et al. Effects of Chitosan Coatings on Polypropylene Mesh for Implantation in a Rat Abdominal Wall Model. *Tissue Eng. Part A*. **00**(00).
115. Iyer S, Udpa N, Gao Y. Chitosan selectively promotes adhesion of myoblasts over fibroblasts. *J. Biomed. Mater. Res. A*. (May 2013), 1, 2013;
116. Klinge U, Si Z, Zheng H, Schumpelick V, Bhardwaj RS, Klosterhalfen B. Collagen I/III and Matrix Metalloproteinases (MMP) 1 and 13 in the Fascia of Patients With Incisional Hernias. *J. Invest. Surg.* **13**, 47, 2001;
117. Hance A, Crystal R. Rigid Control of Synthesis of Collagen Types I and III by Cells in Culture. *Nature*. **268**, 152, 1977;
118. Mays P, Bishop J, Laurent G. Age-related changes in the proportion of types I and III collagen. *Mech. Ageing Dev.* **45**, 1988;
119. Lovell CR, Smolenski K a, Duance VC, Light ND, Young S, Dyson M. Type I and III collagen content and fibre distribution in normal human skin during ageing. *Br. J. Dermatol.* **117**(4), 419, 1987;
120. De Almeida SHM, Rodrigues MAF, Gregório E, Crespígio J, Moreira HA. Influence of sling material on inflammation and collagen deposit in an animal model. *Int. J. Urol.* **14**(11), 1040, 2007;

121. Moalli P a, Debes KM, Meyn L a, Howden NS, Abramowitch SD. Hormones restore biomechanical properties of the vagina and supportive tissues after surgical menopause in young rats. *Am. J. Obstet. Gynecol.* **199(2)**, 161.e1, 2008;
122. Lehto M, Sims TJ, Bailey a J. Skeletal muscle injury--molecular changes in the collagen during healing. *Res. Exp. Med. (Berl).* **185(2)**, 95, 1985;
123. Junge K, Klinge U, Klosterhalfen B, Mertens PR, Rosch R, Schachtrupp a, et al. Influence of mesh materials on collagen deposition in a rat model. *J. Invest. Surg.* **15(6)**, 319, 2002;
124. Goh JTW. Biomechanical and biochemical assessments for pelvic organ prolapse. *Curr. Opin. Obstet. Gynecol.* **15(5)**, 391, 2003;
125. Gao Y, Kostrominova TY, Faulkner J a, Wineman AS. Age-related changes in the mechanical properties of the epimysium in skeletal muscles of rats. *J. Biomech.* **41(2)**, 465, 2008;
126. Rich L, Whittaker P. COLLAGEN AND PICROSIRIUS RED STAINING: A POLARIZED LIGHT ASSESSMENT OF FIBRILLAR HUE AND SPATIAL DISTRIBUTION. *Braz J Morphol Sci.* **22**, 97, 2005;
127. Weyhe D, Belyaev O, Buettner G, Mros K, Mueller C, Meurer K, et al. In vitro comparison of three different mesh constructions. *ANZ J. Surg.* **78(1-2)**, 55, 2008;

128. Pierschbacher MD, Polarek JW, Craig WS, Tschopp JF, Sipes NJ, Harper JR. Manipulation of cellular interactions with biomaterials toward a therapeutic outcome: a perspective. *J. Cell. Biochem.* **56**(2), 150, 1994;
129. Dietz HP. Voiding Function and Dysfunction, Bladder Physiology and Pharmacology, and Female Urology. *J. Urol.* American Urological Association; **182**(1), 229, 2009;
130. Mclean JW. Vaginal prolapse in sheep. *N. Z. Vet. J.* **4**(2), 38, 1956;
131. Scott P, Gessert M. Ultrasonographic Examination of 12 Ovine Vaginal Prolapses. *Vet. J.* (Table I), 323, 1998;
132. Ayen E, Noakes D. Displacement of the tubular genital tract of the ewe during pregnancy. *Vet. Rec.* (1989), 509, 1997;
133. Hilger WS, Walter A, Zobitz ME, Leslie KO, Magtibay P, Cornella J. Histological and biomechanical evaluation of implanted graft materials in a rabbit vaginal and abdominal model. *Am. J. Obstet. Gynecol.* **195**(6), 1826, 2006;
134. Feola A. Impact of vaginal synthetic prolapse meshes on the mechanics of the host tissue response. University of Pittsburgh; 2011.
135. Sacks M. Biaxial mechanical evaluation of planar biological materials. *J. Elast.* **199**, 2000;
136. Sacks M. A Method for Planar Biaxial Mechanical Testing That Includes In-Plane Shear. *J. Biomech. Eng.* **121**(October), 551, 1999;